Universal spectral correlations in the chaotic wave function and the development of quantum chaos

Xiao Chen[1,*] and Andreas W. W. Ludwig[2]
[1]*Kavli Institute for Theoretical Physics, University of California, Santa Barbara, California 93106, USA*
[2]*Department of Physics, University of California, Santa Barbara, California 93106, USA*

(Received 6 July 2018; published 30 August 2018)

We investigate the appearance of quantum chaos in a *single* many-body wave function by analyzing the statistical properties of the eigenvalues of its reduced density matrix $\hat{\rho}_A$ of a spatial subsystem A. We find that (i): the spectrum of the density matrix is described by so-called *Wishart random matrix theory*, which (ii): exhibits besides *level repulsion*, *spectral rigidity*, and *universal spectral correlations* between eigenvalues separated by distances ranging from one up to many mean level spacings, which we investigate. We use these universal spectral characteristics of the reduced density matrix as a definition of chaos in the wave function. A simple and precise characterization of such universal correlations in a spectrum is a segment of strictly linear growth at sufficiently long times, recently called the "*ramp*," of the *spectral form factor* which is the Fourier transform of the *correlation function between a pair of eigenvalues*. It turns out that Wishart and standard random matrix theory have the same universal "ramp." Specifically, here numerical results for the spectral form factor of the density matrix of generic nonintegrable many-body systems, such as one-dimensional quantum Ising and Floquet spin models, are found to exhibit a universal "ramp" identical to that appearing for a *"random pure state"* ("*Page state*," or "Haar state"). The density matrix of the latter is precisely the Wishart random matrix, the reduced density matrix of a completely random wave function. In addition, we study the *development of chaos* in the wave function by letting an initial direct product state evolve under the unitary time evolution. We find that the universal spectral correlations as manifested by the "ramp" set in as soon as the entanglement entropy begins to grow, and first develop for the eigenvalues at the top of the spectrum of the density matrix $\hat{\rho}_A$, subsequently spreading over the entire spectrum at later times. Finally, we study a *prethermalized regime* described by a *generalized Gibbs ensemble*, which develops in a rapidly driven Floquet model at intermediate times. We find that the prethermalized regime exhibits no chaos, as evidenced by the absence of a "ramp" in the spectral form factor of the density matrix, while the universal spectral correlations start to develop when the prethermalized regime finally relaxes at late times to the fully thermalized (infinite temperature) chaotic regime.

DOI: 10.1103/PhysRevB.98.064309

I. INTRODUCTION

The characterization of chaos in quantum mechanical systems has a long history, and chaos plays a key role in the process of thermalization, i.e., relaxation to equilibrium in generic isolated many-body quantum systems [1,2]. (See, e.g., Refs. [3–6] for a review.) It also plays an important role for the quantum nature of black holes [7–12]. An important milestone in the study of quantum chaos has been the so-called *Bohigas, Giannoni and Schmidt conjecture* [13], which states that chaos manifests itself in the spectral properties of the Hamiltonian of a quantum system by exhibiting universal features which are the same as those of the spectrum of a random Hamiltonian matrix in the same symmetry class. Such *universal* features include, besides level repulsion statistics between *adjacent* spectral levels, spectral rigidity and more generally the correlation function between two levels which is universal for levels separated by energy scales that range from the mean level spacing to energy differences which can be much larger, up to scales at which model-dependent ("ultraviolet") features set in. The corresponding universality classes are solely determined by the action of the antiunitary time-reversal operator, giving rise to the three possible symmetry classes of spectral statistics depending on whether time reversal symmetry is absent ("GUE", Dyson index $\beta = 2$), or is present and squares to the identity operator ("GOE", Dyson index $\beta = 1$) or squares to minus the identity operator ("GSE," Dyson index $\beta = 4$).

Spectral characteristics of a discrete spectrum of levels E_i are conveniently described by the so-called *spectral form factor* [14], which is the *Fourier transform* of the *correlation function* between two levels and can be written in the form

$$g(\tau) \equiv \left\langle \sum_{i,j} e^{-i\tau(E_i - E_j)} \right\rangle, \quad (\textit{Spectral Form Factor}). \quad (1.1)$$

Here τ denotes an *auxiliary* real time (*not* to be confused with an 'Euclidean' or 'imaginary' time coordinate, often denoted by the same symbol), and $\langle ... \rangle$ stands for a certain average, to be described in detail below, whose sole purpose is to remove nonuniversal rapid temporal fluctuations (in τ) from the signal which originate from (nonuniversal) high frequency components corresponding to large energy differences $(E_i - E_j)$. In random matrix theory, considering here the simplest case where time-reversal symmetry is absent ("GUE-type"

*xchen@kitp.ucsb.edu

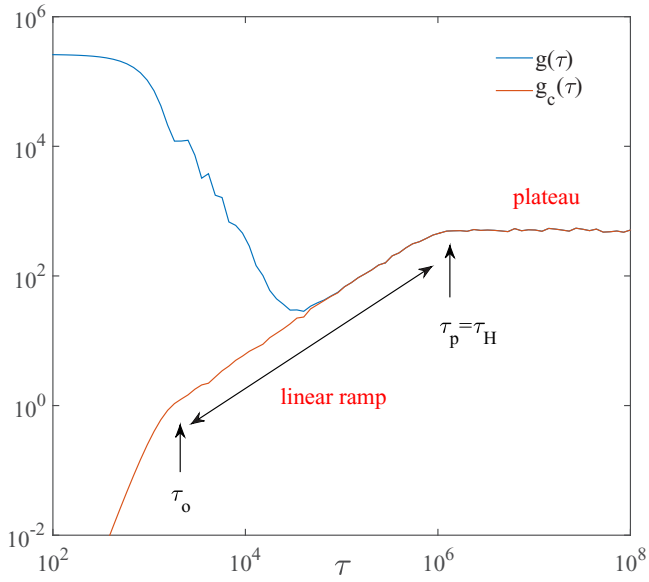

FIG. 1. Typical structure [15] of the linear universal "ramp" in the spectral form factor $g(\tau)$ as well as of the connected spectral form factor $g_c(\tau)$, which exhibits a *longer* "ramp" ranging from a microscopic short time scale τ_0 below which nonuniversal effects set in, up to the Heisenberg time τ_H (also called plateau time τ_p).

statistics), a simple and precise characterization of universal spectral correlations is a *segment of strictly linear growth* [15] in time τ, recently called [12] the "*ramp*," of the spectral form factor $g(\tau)$ at sufficiently long times up to the so-called Heisenberg time τ_H (defined to be 2π times the inverse of the mean level spacing), where it suddenly becomes completely flat, reaching its long-time "plateau" value, as sketched [16] in Fig. 1. [The Heisenberg time has also been called "plateau time" $\tau_p \equiv \tau_H$.] More precisely, the *connected* spectral form factor $g_c(\tau)$ obtained [17] from (1.1) by subtracting a (nonuniversal) disconnected piece $|\langle\sum_i e^{-i\tau E_i}\rangle|^2$, turns out to exhibit a longer segment of universal, strictly linear growth ("ramp") for time scales τ larger than a shortest time scale τ_0 below which (in applications, e.g., to spectra of Hamiltonians describing quantum chaos) possible nonuniversal features set in. I.e., the region $\tau \lesssim \tau_0$ corresponds to differences of energies $(E_i - E_j)$ which exceed the universal regime. In the (nonconnected) spectral form factor $g(\tau)$ from (1.1), a portion of this universal segment of linear growth in $g_c(\tau)$ turns out to be hidden at small times larger than τ_0 by possible nonuniversal features of the disconnected part, and $g(\tau)$ typically only exhibits a shorter part of the entire universal linear "ramp," as depicted in Fig. 1.

It was shown [18,19] many years ago that in chaotic quantum systems with a small number of degrees of freedom whose classical limit is ergodic, the "ramp" for the energy spectrum of the Hamiltonian can be computed analytically in the semiclassical limit by making use of Gutzwiller's Trace Formula [20] and known properties of asymptotically long classical periodic orbits. In these cases, the time-scale τ_0 characterizes the onset of potential nonuniversal contributions to $g_c(\tau)$ for $\tau \lesssim \tau_0$ arising from short orbits. On the other hand, the spectral form factor has very recently formed a topic of extensive discussion in the context of the Sachdev-Ye-Kitaev (SYK) model [21–23], a strongly chaotic quantum system, whose Hamiltonian has been shown numerically to exhibit a spectrum possessing the expected "ramp." A recent lucid discussion of many aspects of the spectral form factor, with an emphasis on the Hamiltonian spectrum of the SYK model, can be found in Ref. [12]. In contrast, these universal spectral correlations are absent in an integrable system, where the spectral form factor exhibits no "ramp" (and the probability distribution for the spacing between adjacent levels is Poissonian).

In the present paper, we are going to show that the universal spectral correlations manifested by a strictly linear "ramp" already appear at the level of a single many-body wave function of a generic chaotic quantum system, without focusing attention on the spectrum of the Hamiltonian of the system; we also discuss periodically driven Floquet systems.

For thermalizing (chaotic) systems whose time evolution is governed by a time-independent Hamiltonian (i.e., not Floquet systems), our work can be motivated by the connection between a typical state and the thermal ensemble, a notion inherent in the eigenstate thermalization hypothesis [1,2] (ETH), which we now briefly summarize as follows: Let $|\psi\rangle$ be a state at finite energy density $e = E/V$ (i.e., $\langle\psi|\hat{H}|\psi\rangle = E = e\,V$, where V is the volume), which can either be a highly excited exact eigenstate of a chaotic Hamiltonian $\hat{H}$ in the spatial volume V, or just a typical short-range entangled initial state (which is not an eigenstate of $\hat{H}$) acted on by the corresponding unitary quantum mechanical time-evolution operator for a sufficiently long time. ETH states that the expectation value of a product of local operators in the state $|\psi\rangle$ equals the thermal expectation value of this product at a temperature determined by e in the usual sense of microcanonical statistical mechanics. For Floquet systems, these expectations values in the analogous state $|\psi\rangle$ are at infinite temperature.

Here we consider the reduced density matrix in a spatial subregion A ($B = \bar{A}$ is the complement of A) of such a typical state,

$$\hat{\rho}_A = \mathrm{Tr}_B\, |\psi\rangle\langle\psi|. \tag{1.2}$$

We will show that the spectral form factor for the spectrum of eigenvalues λ_i of the reduced density matrix $\hat{\rho}_A$,

$$g(\tau) \equiv \left\langle \sum_{i,j} e^{-i\tau(\lambda_i - \lambda_j)} \right\rangle, \tag{1.3}$$

exhibits a "ramp." As mentioned above, the presence of a "ramp" in the spectral form factor demonstrates the presence of universal spectral correlations over a possibly large range of scales (determined by τ_0 and τ_H) in the spectrum of eigenvalues of the density matrix. Thus, in this paper we use the presence of these universal spectral correlations in the spectrum of eigenvalues of the reduced density matrix of a typical quantum state $|\psi\rangle$, as manifested by the presence of a "ramp" in the associated spectral form factor, to define the notion of quantum chaos in the state (i.e., "in the wave function"). In particular, we will show at the technical level that spectral properties of the reduced density matrix $\hat{\rho}_A$ are described by so-called *Wishart random matrix theory* [24]. As it turns out, Wishart random matrix theory exhibits universal spectral correlations identical to those appearing in standard (here [25] GUE) random matrix

theory; in particular they have the same universal linear "ramp" (see Sec. IV C and Appendix B).

For systems whose time evolution is governed by a time-independent Hamiltonian, we can look at this also from a slightly different angle: Instead of investigating the spectral statistics of the reduced density matrix, one may also be inclined to consider the spectral statistics of the associated entanglement Hamiltonian $\hat{H}_E$ defined by

$$\hat{\rho}_A = \mathcal{N}_E^{-1} \exp\{-\beta_{\text{eff}} \hat{H}_E\}. \tag{1.4}$$

The spectral form factor for the entanglement Hamiltonian is obtained from (1.3) by letting $\lambda_i \to -\ln \lambda_i$. As discussed in Appendix A, the two spectral form factors, of $\hat{\rho}_A$ and of $\hat{H}_E$, exhibit identical universal features in their respective level statistics. In particular, in a chaotic system they both exhibit a linear "ramp." Now, one may think of the entanglement Hamiltonian and of (1.4) in the light of a strong version of ETH proposed in Ref. [26], which states that the reduced density matrix of the single state $|\psi\rangle$ takes on a thermal form, $\hat{\rho}_A = \mathcal{N}_A^{-1} \exp\{-\beta \hat{H}_A\}$, where $\hat{H}_A$ is the physical (chaotic) Hamiltonian of the system, projected onto the region of subsystem A. Note that this strong version of ETH [26] is a quite nontrivial statement because even though $\hat{\rho}_A$ is constructed from a *single* state [see (1.2)], this statement implies that $\hat{\rho}_A$ contains the knowledge of the *entire* Hamiltonian of the system, or rather at least of its projection onto A. Then, if one assumes the validity of the above-mentioned strong version of ETH, one would naturally expect that the universal correlations in the spectrum of the entanglement Hamiltonian $\hat{H}_E$ are directly inherited from those of the physical Hamiltonian $\hat{H}_A$ (which, according to the Bohigas, Giannoni, and Schmidt conjecture, is expected to exhibit universal spectral correlations). Thus, since we observe (as mentioned) that $\hat{\rho}_A$ and $\hat{H}_E$ exhibit the same universal features in their spectral form factors, it would be natural to expect the appearance the universal spectral correlations (and the "ramp") in the entanglement Hamiltonian of a single state $|\psi\rangle$. Put another way, for thermalizing (chaotic) systems whose time evolution is governed by a time-independent Hamiltonian, our results can thus also be viewed as a confirmation of the strong version of ETH proposed in Ref. [26].

In order to investigate explicitly the presence of the mentioned universal correlations in the spectrum of the reduced density matrix (1.2) in many-body quantum chaos, we numerically compute the spectral form factor of the density matrix of a typical *single* many-body wave function $|\psi\rangle$ [as defined in the paragraph above (1.2)], in two generic nonintegrable one-dimensional systems: a Floquet spin model and a quantum Ising model in both transverse and longitudinal field. As will be shown below in the bulk of the paper, we clearly observe for both systems a linear "ramp" in the spectral form factors of their density matrices, confirming the corresponding universal spectral correlations in their spectra of eigenvalues. Furthermore, in order to provide a generic, model-independent description of the universal features of quantum chaos in a wave function, we consider a so-called "random pure state," or "Page state" ("Haar state") [27],

$$|\Psi(\{\alpha_i\})\rangle = \sum_i \alpha_i \, |C_i\rangle, \tag{1.5}$$

in which the coefficients α_i of the state in a fixed basis $\{|C_i\rangle\}_i$ are random complex numbers subject solely to the normalization constraint, with a probability distribution invariant under unitary basis changes. The set of coefficients $\{\alpha_i\}_i$ can thus be considered a row (or column) vector of a unitary random matrix (distributed according to the Haar measure). When we now form the reduced density matrix $\hat{\rho}_A$ of the "random pure state" (1.5) in a spatial region A, we obtain a random matrix which turns out to belong to the well-studied "Wishart random matrix ensemble" (see Sec. IV A below for a more detailed discussion). The probability distribution for the eigenvalues of the Wishart random matrix and hence of the density matrix $\hat{\rho}_A$ of the "random pure state" are known analytically (as reviewed in Sec. IV B), and the spectral form factor for $\hat{\rho}_A$ can be shown analytically (see Sec. IV C and Appendix B) to exhibit a linear "ramp" in the limit of large density matrices, reflecting the presence of universal spectral correlations in their spectra. As already mentioned, the linear "ramp" in $g_c(\tau)$ for the eigenvalues of the Wishart random matrix turns out to be identical to that of standard random matrix theory in the same symmetry class (see Sec. IV C and Appendix B). The spectral form factor for the "random pure state" is discussed in detail in Sec. II B below. In Sec. II C we compare the numerically obtained spectral form factors of the Floquet and the quantum Ising systems with that of the "random pure state" (for the same system sizes) and find full agreement of the universal features. This means that Wishart random matrix theory describes the spectral correlations of the reduced density matrix of a single many-body wave function in typical chaotic systems of Hamiltonian and Floquet type in their universal regime, just as ordinary random matrix theory is thought to describe the level statistics of a chaotic Hamiltonian (according to the Bohigas, Giannoni, and Schmidt conjecture [13]). The Floquet and quantum Ising systems considered in this paper lack time-reversal symmetry and so the "GUE" Wishart random matrix ensemble will be appropriate.

Subsequently, we explore the important question of development of quantum chaos under quantum mechanical unitary time evolution. Recently, it has been proposed that the "out-of-time-ordered" correlation function (OTOC) can probe the development of chaotic dynamics and scrambling of quantum information [7–11,28]. At early times, the OTOC can exhibit an exponentially growing regime, the growth rate of which represents a quantum analog of the (classical) Lyapunov exponent. In this paper, we will study instead as an indicator of the development of quantum chaos the emergence of universal spectral correlations and of the corresponding "ramp" in the spectral form factor, in the spectrum of the reduced density matrix $\hat{\rho}_A(t)$ as a function of time t in a quantum quench problem. ETH states that an (sufficiently general short-range entangled) initial state which is not an eigenstate, relaxes under the quantum mechanical time evolution, after a sufficiently long time, to a state which appears to be (in the sense of ETH, as reviewed above) in thermal equilibrium (at infinite temperature for Floquet systems) [1,2]. Therefore, if we start with an initial direct product state, one expects that while the spectrum of the reduced density matrix $\hat{\rho}_A(t)$ will initially exhibit no spectral correlations, under the unitary time evolution a "ramp" will emerge after a sufficiently long time t in its spectral form factor. We consider both (one-dimensional) Floquet and quantum

Ising models and find that a "ramp" starts to develop as soon as the entanglement entropy begins to grow. More precisely, it is interesting to note that universal spectral correlations are first seen to appear for the eigenvalues at the top of the spectrum of the reduced density matrix $\hat{\rho}_A(\mathrm{t})$, and subsequently spread out over the entire spectrum at later times.

We emphasize that there is no direct connection between the appearance of a volume law in the entanglement entropy and quantum chaos. In integrable systems, initial direct product states (as above) are typically expected to thermalize to a generalized Gibbs ensemble (GGE) after sufficiently long unitary time evolution [29–32]. Although the reduced density matrix $\hat{\rho}_A$ for these GGE states possesses an entanglement entropy exhibiting a volume law, the eigenvalues of this density matrix are not expected to exhibit the discussed universal spectral correlations, in contrast to the reduced density matrix of chaotic (thermalizing) systems discussed above. To illustrate this point explicitly, we have constructed a rapidly driven Floquet system whose time evolution, starting out from a direct product state, exhibits a long, stable so-called prethermalized regime [33–36] at intermediate times. This prethermalized regime, accompanied by a long plateau in the time dependence of the entanglement entropy exhibiting a volume law, will be seen to be clearly devoid of chaos as evidenced from the absence of the characteristic universal spectral correlations in the spectrum of the density matrix $\hat{\rho}_A(t)$, which is manifested by the absence of a "ramp" in the corresponding spectral form factor. A linear "ramp" in the spectral form factor is seen to develop only when the prethermalized regime eventually relaxes at very late times to the fully thermalized chaotic regime, in which the conservation laws (approximately) present in the prethermalized regime cease to exist.

We end the introduction by mentioning some related work. Level repulsion statistics between adjacent levels of the density matrix of thermalizing systems with a main focus on disordered systems has been discussed in the context of work investigating Many-Body-Localization (MBL) in Refs. [37] and [38]. Level repulsion statistics and level variance of the reduced density matrix of a spinless Hubbard model, subject to a constant electric field and after a flux quench, was discussed in Ref. [39]. Our work, in contrast, discusses spectral rigidity and, in particular, the universal spectral correlations and the "ramp" in the spectral form factor, focusing on non-random chaotic systems, and it elucidates the origins of these spectral correlations in the "random pure state" (Page state) and in Wishart random matrix theory, both for Hamiltonian and Floquet systems. Furthermore, we identify the *development of chaos* as the process of buildup of these spectral correlations in the density matrix under the unitary time-evolution. We also discuss a prethermal regime, lacking chaos, and its late-time relaxation to a chaotic state.

The rest of the paper is organized as follows. In Sec. II, we first discuss the spectral form factor in the "random pure state" (Page state) and its linear "ramp." Then, we discuss the spectral form factors of typical wave functions of nonintegrable Floquet and quantum Ising models for the same system sizes and show that they both exhibit the same universal linear "ramp" as the "random pure state." In Sec. III, we discuss the development of chaos in these Floquet and Ising model wave functions by computing the time evolution of the spectral form factor. Moreover, we explore the development of chaos in a Floquet model which exhibits a long prethermal regime at intermediate times. In Sec. IV, we compute the spectral form factor in the "random pure state" (Page state) analytically by using some basic knowledge of the Wishart ensemble and compare the result with the numerical calculations in Sec. II. We summarize and conclude in Sec. V.

II. SPECTRAL FORM FACTOR

A. General discussion

We decompose the Hilbert space of the total system of dimension N (of which the "typical" state $|\psi\rangle$ is an element) into a tensor product of the Hilbert spaces of the two subsystems, system A with Hilbert space dimension N_A, and system B with Hilbert space dimension N_B (i.e., $N = N_A N_B$). The spectral form factor $g(\tau)$ for the N_A eigenvalues λ_i of the reduced density matrix $\hat{\rho}_A$ defined in (1.3) above can be conveniently expressed [40] in terms of the Fourier transform of the eigenvalue density

$$Z(\tau) \equiv \mathrm{Tr}\ \exp(-i\tau\hat{\rho}_A) = \sum_{i=1}^{N_A} \exp(-i\tau\lambda_i) \tag{2.1}$$

as follows

$$g(\tau) = \left\langle \sum_{i,j=1}^{N_A} e^{-i\tau(\lambda_i-\lambda_j)} \right\rangle = \langle Z(\tau)Z^*(\tau)\rangle. \tag{2.2}$$

As seen from (2.2), at $\tau = 0$ the spectral form factor clearly takes on the value $g(\tau = 0) = (N_A)^2$, while in the limit $\tau \to \infty$ only contributions with $\lambda_i = \lambda_j$ survive, which yields the smaller value $\lim_{\tau\to\infty} g(\tau) = N_A$. As we will see below, the function $g(\tau)$ initially *decreases* starting from $\tau = 0$ until it reaches a minimum ("dip"), then exhibits a segment of linear rise ("ramp"), until the curve suddenly becomes constant (at the Heisenberg time τ_H) reaching its late-time "plateau" value (see, e.g., Fig. 1). As we will review below, the initial *decrease* at early times is nonuniversal, whereas the linear "ramp" is completely universal, depending only on the symmetry class. We note that the presence of these three distinct regimes, the decrease until the "dip," the linear rise along the "ramp," and the flat plateau, was stressed in the context of the spectral form factor of the *Hamiltonian* of the SYK model in the recent Ref. [12] already mentioned above.

We will also consider the connected spectral form factor

$$g_c(\tau) = \langle Z(\tau)Z^*(\tau)\rangle - \langle Z(\tau)\rangle\,\langle Z^*(\tau)\rangle, \tag{2.3}$$

which exhibits (as already mentioned) a longer and more pronounced "ramp" (compare, e.g., Fig. 1). Its analytic form for the "random pure state" and the Wishart random matrix ensemble is displayed in (4.24) of Sec. IV in the limit of a large density matrix. In the context of the spectrum of a random (GUE, GOE, or GSE) Hamiltonian matrix, the connected spectral form factor $g_c(\tau)$ has been extensively discussed in the literature over many years [41].

As already mentioned in the Introduction (Sec. I), the purpose of the average $\langle\ldots\rangle$ in (2.2) and (2.3) is to remove nonuniversal rapid temporal fluctuations [42] from the spectral form factor $g(\tau)$. In our work reported below, there will be a

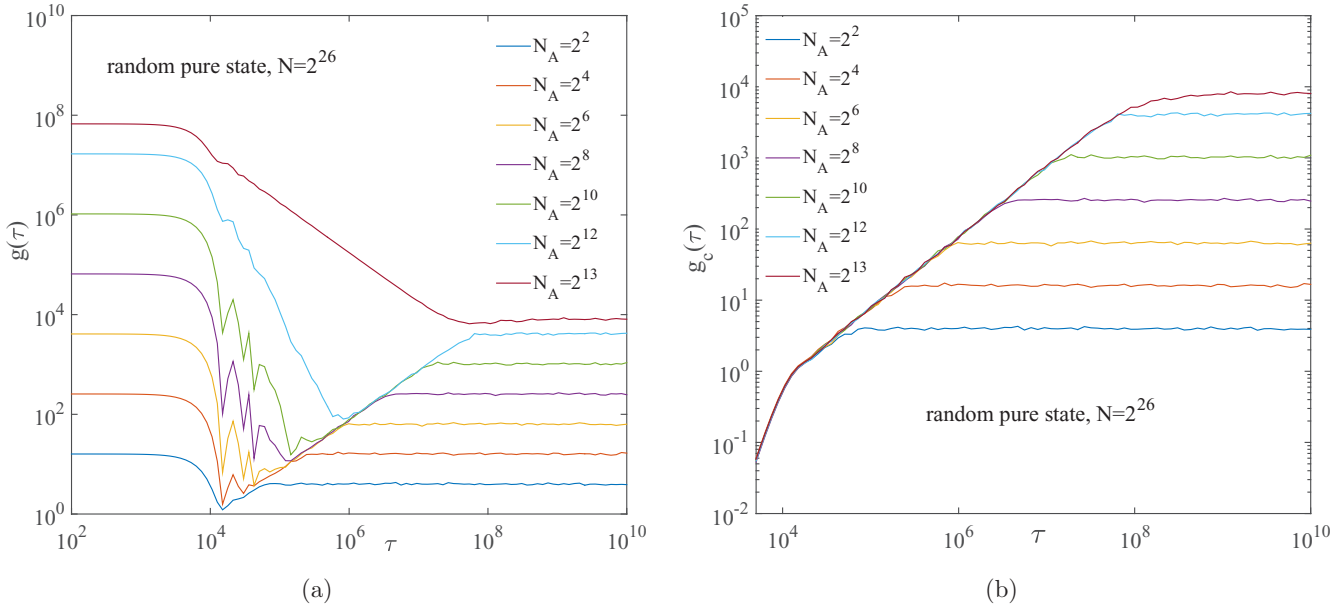

FIG. 2. (a) Spectral form factor $g(\tau) = \langle ZZ^* \rangle$ for the "random pure state" (Page state) with fixed value of $N = 2^L$ and different values of $N_A = 2^{L_A}$, where L is the total number of lattice sites, and L_A denotes the number of lattice sites in subsystem A. The curve is obtained by taking the disorder average over 1000 states. (b) Connected spectral form factor $g_c(\tau) = \langle ZZ^* \rangle - \langle Z \rangle \langle Z^* \rangle$ for the "random pure state" with fixed values of N and different values of N_A. Again, the curve is obtained by taking the disorder average over 1000 states.

natural ensemble available over which to perform the average as an *ensemble average*: For the "random pure state" (Page state) discussed in Sec. II B below, this will be an average over the statistical ensemble of "random pure states," while for the Floquet and quantum Ising models in Sec. II C this will be an ensemble of initial direct product states. Another way to remove the high-frequency fluctuations from the spectral form factor $g(\tau)$ is to coarse grain the latter in time τ by convolution with a temporal "smearing function" which eliminates high frequencies components from the signal. (For example, see Refs. [12,43].) Since the ensemble averages were more convenient for us, we did not use the coarse graining approach in the present work to remove the high frequency fluctuations.

B. Random pure state

Since, as already mentioned in the Introduction, this will turn out to provide a model-independent description of the universal properties of quantum chaos in a wave function, we first study the spectral form factor of the "random pure state" (Page state), discussed in (1.5) and the paragraph below that equation. The reduced density matrix for a "random pure state" is also a random matrix and it turns out to belong to the so-called (unitary) Wishart ensemble with Dyson index $\beta = 2$, in which the spectral density satisfies the so-called Marchenko-Pastur distribution [24]. (See Sec. IV for a review.)

Using this property, Page showed [27] that the ensemble-averaged (von Neumann) entanglement entropy [EE] of the reduced density matrix for subsystem A of the "random pure state" is equal to

$$\langle S_A \rangle = \log N_A - \frac{N_A}{2N_B}. \tag{2.4}$$

(Recall that N_A and N_B are Hilbert space dimensions for subsystem A and its complement B, respectively, and we have assumed $N_A \leqslant N_B$ without loss of generality.)

Since the Hilbert space dimension N_A grows exponentionally with the volume of subsystem A, the entanglement entropy of the random product state exhibits according to (2.4) a volume law (as expected). For example, for the Ising-type systems considered in the present paper which have a local (onsite) Hilbert space dimension of two, we have $N_A = 2^{L_A}$ where L_A is the number of lattice sites of subsystem A. We thus seen from (2.4) that the entanglement entropy of the "random pure state" exhibits a volume law of maximal possible value (given the dimension of the onsite Hilbert space), up to a small subleading term which depends on the ratio of the Hilbert space dimensions of subsystems A and B, which we denote by $\alpha \equiv N_A/N_B$. The latter subleading term in (2.4) takes on its maximal value $1/2$ at $\alpha = 1$ and approaches zero as $N_A \ll N_B$.

It it known analytically (as reviewed in Sec. IV below) that the eigenvalues of the Wishart random matrix exhibit the same universal spectral correlations as those of the Hamiltonian of the GUE random matrix ensemble, which manifest themselves, as already mentioned, in the *connected* spectral form factor $g_c(\tau)$. We have computed numerically the (nonconnected) spectral form factor $g(\tau) = \langle Z(\tau)Z^*(\tau) \rangle$ for the eigenvalues of the Wishart random matrix, describing the reduced density matrix of the "random pure state." The results are plotted in Fig. 2(a) which shows that when $\alpha = N_A/N_B < 1$, there is an intermediate linear "ramp" where $g(\tau) = \langle Z(\tau)Z^*(\tau) \rangle$ grows linearly with time τ. The presence of the "ramp" demonstrates the presence of the mentioned universal spectral correlations, as discussed analytically in Sec. IV below (compare also Fig. 1).

Continuing with $\alpha = N_A/N_B < 1$, we also observe in Fig. 2(a) an early time regime where $g(\tau) = \langle Z(\tau)Z^*(\tau) \rangle$

drops down quickly to a minimum value. It turns out that at early times, $\langle Z(\tau)Z^*(\tau)\rangle$ factorizes into $\langle Z(\tau)\rangle\langle Z^*(\tau)\rangle$ and is therefore determined by the Fourier transform of the average of the eigenvalue density, $\langle Z(\tau)\rangle$, defined in (2.1). One can determine from Fig. 2(a), where $g(\tau) = \langle Z(\tau)Z^*(\tau)\rangle$ is plotted versus τ for $N_A = 2^{12}$ (and $N = 2^{26}$, i.e., when $\alpha = 1/4$), that it scales as $1/\tau^3$ in this early time regime. Moreover, we observe in the plots shown in the same figure for smaller values of α, that there are large oscillations in this early time regime [44], but with an envelope function that is still close to $1/\tau^3$, when compared to the $\alpha = 1/4$ case.

This power law decay behavior of the spectral form factor at early times originates from the eigenvalue distribution function $\langle Z(\tau)\rangle$ of the Wishart matrix which will be analytically computed in Sec. IV B. For a generic chaotic system with Hamiltonian $\hat{H}$, the details of the eigenvalue distribution function of the density matrix $\hat{\rho}_A$ for a typical wave function will in general be different from that of the Wishart matrix, and will not be universal. In particular, in the early time regime where the spectral form factor $g(\tau) = \langle Z(\tau)Z^*(\tau)\rangle$ factorizes into $\langle Z(\tau)\rangle\langle Z^*(\tau)\rangle$, it will be model dependent, in contrast to the regime of intermediate τ where it exhibits a universal "ramp," whose presence depends solely on the universal spectral correlations in the spectrum of eigenvalues.

As already discussed, at late times τ larger than the Heisenberg time τ_H, the spectral form factor $g(\tau) = \langle Z(\tau)Z(\tau)^*\rangle$ will saturate to a constant value N_A, which is coming from the terms with $\lambda_i = \lambda_j$ [see (2.2)]. Since, as has also been mentioned, the saturation value is much smaller than the initial value N_A^2 attained at $\tau = 0$ [see again (2.2)], we plot $g(\tau) = \langle Z(\tau)Z^*(\tau)\rangle$ on a log-log scale so that the behavior of $\langle ZZ^*\rangle$ at the different time scales τ can be seen clearly. The three time regimes mentioned in Sec. (II A) are separated by two typical time scales: The time where the "dip" occurs ("dip time") τ_d, and the time where the plateau begins ("plateau time," or "Heisenberg time") $\tau_p = \tau_H$. We find that the dip time τ_d scales as $\sqrt{N_A N}$, while τ_p is found to scale as $N_A\sqrt{N}$. (Recall $N = N_A N_B$.) (Both statements are obtained analytically in Sec. IV and have also been checked numerically.) This is analogous to the three regimes observed in Ref. [12] for the spectral form factor for a $M \times M$ random matrix in the GUE ensemble (as compared to the Wishard random matrix ensemble discussed here), where $\tau_d \sim \sqrt{M}$ and $\tau_p \sim M$.

We finally discuss a subtlety occurring when $\alpha = N_A/N_B = 1$. In contrast to the case where $\alpha < 1$ discussed above, we see from Fig. 2(a) (top curve, $N_A = 2^{13}$, where the total Hilbert space dimension is $N = 2^{26}$) that for $\alpha = 1$ the intermediate "ramp" in $g(\tau)$ disappears. The difference between $\alpha = 1$ and $\alpha < 1$ is caused by the different behavior of $\langle Z(\tau)\rangle$: At early times, where $g(\tau) = \langle Z(\tau)Z^*(\tau)\rangle \sim \langle Z(\tau)\rangle\langle Z^*(\tau)\rangle$ factorizes, for $\alpha = 1$ the spectral form factor scales as $1/\tau$ and then directly transits to the plateau. However, the absence of the "ramp" does not mean that universal spectral correlations are absent in the spectrum of eigenvalues when $\alpha = 1$. Rather, the different behavior of $\langle ZZ^*\rangle$ just turns out to *hide* the "ramp" due to the slow decay of the disconnected part $\langle Z(\tau)\rangle\langle Z^*(\tau)\rangle$. The effect of the slowly decaying $\langle Z(\tau)\rangle$ can be removed if we consider instead the connected spectral form factor $g_c(\tau) = \langle ZZ^*\rangle - \langle Z\rangle\langle Z^*\rangle$, which is plotted in Fig. 2(b). In the latter figure we observe a long "ramp" *even* for $\alpha = 1$. Actually, for the other curves with $\alpha < 1$ in the same figure, the linear "ramp" in $g_c(\tau)$ starts at an earlier time (denoted earlier by τ_0, see Fig. 1) than the "ramp" in $g(\tau)$, where part of the longer linear "ramp" in $g_c(\tau)$ is in fact covered up by $\langle Z\rangle\langle Z^*\rangle$ as depicted in Fig. 2(a). Since small values of τ correspond to large eigenvalue differences on the scale of the mean level spacing, the early-time part $\tau_0 \leqslant \tau \ll \tau_H$ of the "ramp" in $g_c(\tau)$ describes the spectral correlations of eigenvalues separated by an energy scale of many times the mean level spacing. Eventually, as τ is close to τ_0, the universal behavior of $g_c(\tau)$ reflected in the linear "ramp" will be limited by model-dependent ("ultraviolet") effects at large separations of eigenvalues, leading to deviations from the linear "ramp" at yet smaller values of $\tau \lesssim \tau_0$.

The length of the "ramp" in $g(\tau)$ increases with the number of eigenvalues that exhibit universal spectral correlations [12]. We clearly see from Fig. 2(b) that both the length of "ramp," and the position of τ_p, are linearly proportional (on a log scale) to $\log N_A$.

We finally want to mention that the reduced density matrix $\hat{\rho}_A$ studied in this section belongs to the Wishart random matrix ensemble *lacking time-reversal symmetry*, described by Dyson index $\beta = 2$ (i.e., the "GUE-type" version of the Wishart random matrix ensemble). We can also consider a density matrix $\hat{\rho}_A$ described by a Wishart ensemble with Dyson index $\beta = 1, 4$ (the "GOE" and the "GSE" version of the Wishart random matrix ensemble), in which the details of the universal spectral correlations are slightly different. In the spectral form factor, these modified spectral correlations between the eigenvalues are reflected in a similar but slightly more complicated universal "ramp." [24] While a straightforward extension, we will not discuss details of these cases explicitly in this paper.

C. Floquet and quantum Ising models

For a generic chaotic system with a time-independent Hamiltonian $\hat{H}$, we expect that for the states $|\psi\rangle$ with energy expectation value E ($=\langle\psi|\hat{H}|\psi\rangle = eV$, where e is the energy density) in the middle of the spectrum of $\hat{H}$, the resulting density matrix $\hat{\rho}_A$ of the subsystem is well thermalized and its entanglement entropy exhibits a volume law. As already mentioned in the introduction, one might expect based on notions from ETH that the spectrum of this reduced density matrix exhibits universal spectral correlations. In this section, we will show more specifically for both one-dimensional Floquet and quantum Ising models that the spectra of the reduced density matrices of the above-mentioned states $|\psi\rangle$ have the same universal properties as those of the "random pure states" (Page states), and that the universal features of their reduced density matrix are in fact those of the Wishart random matrix, which is the reduced density matrix of the "random pure state," the density matrix of a completely random wave function.

For practical reasons, instead of diagonalizing the Hamiltonian (or the Floquet operator) to investigate the spectral statistics the reduced density matrix obtained for the subsystem for a typical *eigenstate* [45], we will choose a set of initial product states $|\Psi_0\rangle$ (which thus are not entangled) and let them evolve under the unitary evolution governed by the Floquet

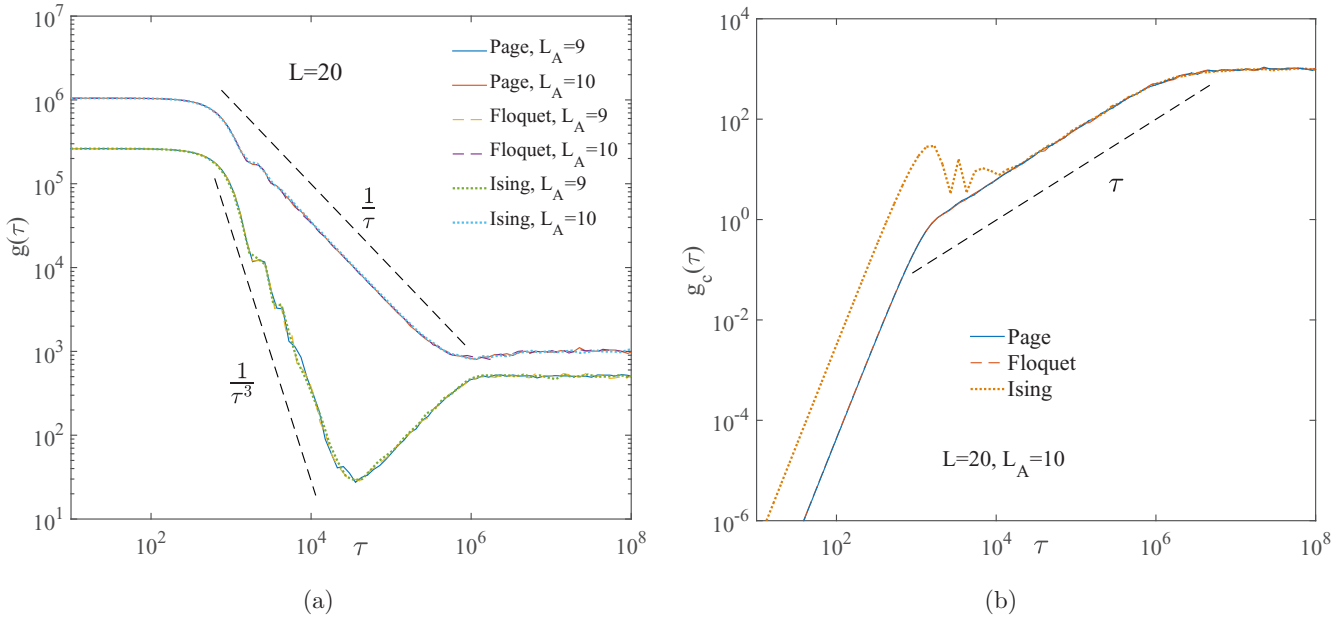

FIG. 3. (a) $g(\tau) = \langle ZZ^* \rangle$ for Page state, Floquet, and quantum Ising models. (b) $g_c(\tau) = \langle ZZ^* \rangle - \langle Z \rangle \langle Z^* \rangle$ for Page state, Floquet, and quantum Ising models. For both (a) and (b), we average over an ensemble containing over 1000 states.

operator or Ising Hamiltonian, i.e.,

$$|\Psi_0(t)\rangle = U(t)|\Psi_0\rangle. \tag{2.5}$$

This is actually a quantum quench problem. For a generic nonintegrable system, the initial wave function $|\Psi_0\rangle$ will eventually, at long times t, thermalize under its own dynamics and the reduced density matrix $\hat{\rho}_A(t) = \mathrm{Tr}_B |\Psi_0(t)\rangle\langle\Psi_0(t)|$ will approach the reduced density matrix of a generic eigenstate of the Hamiltonian [1,2]. Universal spectral correlations will develop in the spectrum of the reduced density matrix starting from such unentangled initial states, so that the final state obtained after sufficiently long time evolution will be fully thermalized. The advantage of this method is that we can work with relatively large systems (the time evolution operator simply has to be applied for a long time). Specifically, we will consider below one-dimensional Floquet and Ising models with $L = 20$ lattice sites.

1. *Floquet model*

We first consider a Floquet model. It is known that Floquet systems can thermalize very rapidly due to the absence of any conservation laws [6,46–49]. The properties of such periodically driven systems are determined by the unitary time evolution operator over one period, i.e., the Floquet operator. Following Ref. [46], we consider the following Floquet operator

$$\hat{U}_F = \exp[-it_0 \hat{H}_z] \exp[-it_0 \hat{H}_x], \tag{2.6}$$

where

$$\hat{H}_x = \sum_{j=1}^{L} g \hat{\sigma}_j^x$$

$$\hat{H}_z = \sum_{j=1}^{L-1} \hat{\sigma}_j^z \hat{\sigma}_{j+1}^z + \sum_{j=1}^{L} h \hat{\sigma}_j^z, \tag{2.7}$$

and $\hat{\sigma}_j^x$ and $\hat{\sigma}_j^z$ are standard Pauli matrices acting on lattice site j. This model is a one-dimensional periodically driven system with period $T = 2t_0$. In the numerical calculations discussed below we choose open boundary conditions and typical system parameters $(g, h, t_0) = (0.9045, 0.8090, 0.8)$. We choose a set of initial states which are random product states (hence unentangled, having vanishing EE) with the direction of the spin at each lattice site chosen independently from a uniform distribution on the Bloch sphere.

Since we are considering a Floquet model, the evolution time t is an integer multiple of T, i.e., $t = nT$ with $n \in \mathbb{Z}_+$. For the parameters we are considering here, it only takes a small number of time steps to achieve thermalization. The details of the thermalization process itself and of the development of chaos will be discussed in Sec. III below. Here we discuss the properties of the fully thermalized state that the system takes on after sufficiently long time evolution. Note that since for a Floquet system energy is not conserved, one expects that the subsystem ($L_A \leqslant L/2$) will always thermalize to a state at infinite temperature close to the "random pure state" discussed above [49].

In Fig. 3 we present numerical results for the spectral form factor $g(\tau) = \langle Z(\tau) Z^*(\tau) \rangle$ and for the connected spectral form factor $g_c(\tau) = [\langle Z(\tau) Z^*(\tau) \rangle - \langle Z(\tau) \rangle \langle Z^*(\tau) \rangle]$ at time step $n = 30$, when the system is fully thermalized. We see from Fig. 3 that for both $L_A = 9$ and for $L_A = 10$ [here $L = 20$], both quantities $g(\tau)$ and $g_c(\tau)$ are indistinguishable from those for the "random pure state." The "ramp" in $g(\tau) = \langle Z(\tau) Z^*(\tau) \rangle$ is absent when $L_A = 10 = L/2$, but becomes visible once we subtract the disconnected part $\langle Z(\tau) \rangle \langle Z^*(\tau) \rangle$ to obtain the connected spectral form factor $g_c(\tau)$ (as discussed above in the context of the "random pure state").

We also note that there is another way to generate an ensemble that can be used to perform the average: We can pick a *fixed initial state* $|\Psi_0\rangle$, but consider an ensemble of states whose members consist of the *time series of states* originating

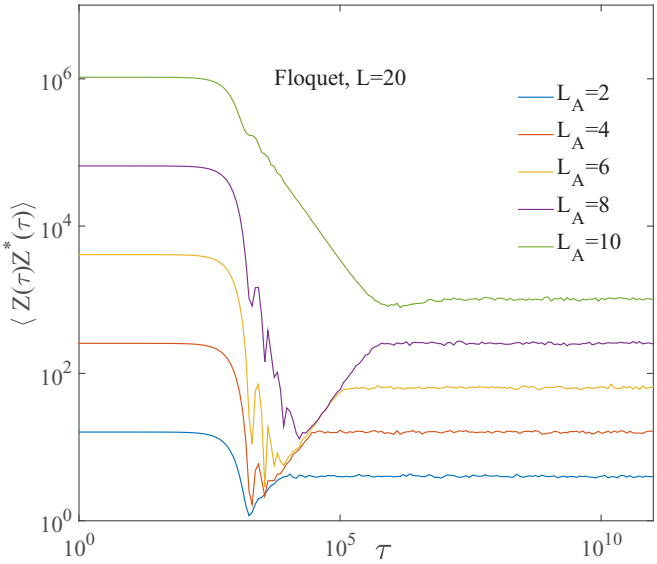

FIG. 4. Spectral form factor averaged over a time series of 1000 states $|\Psi_0(t_m)\rangle$ generated from a single initial product state [see (2.8)] at times $t_m = T_0 + m\ \delta t$, where $T_0 = 40$ is chosen sufficiently large to ensure the initial state has already thermalized.

from the time evolution of this *fixed* state by different amounts of time $t_m \equiv T_0 + m\ \delta t$, where T_0 is a large time ensuring that the initial state has "thermalized," δt is some time step ($= T$ in the Floquet case), and $m = 1, 2, \ldots, M$, i.e.

$$|\Psi_0(t_m)\rangle = \hat{U}(t_m)|\Psi_0\rangle, \quad (m = 1, \ldots, M). \tag{2.8}$$

In this situation the time average over the set of states (2.8) at times t_m then generates the ensemble average of the spectral form factor. The resulting averaged spectral form factor is displayed in Fig. 4 and seen to exhibit the same universal linear "ramp" as that arising from averaging over the ensemble of initial states $|\Psi_0\rangle$ displayed in Fig. 3.

2. Quantum Ising model

In this section we study the transverse field quantum Ising Hamiltonian with a longitudinal field. The Hamiltonian is

$$\hat{H} = \sum_i \hat{\sigma}_i^z \hat{\sigma}_{i+1}^z + h_x \sum_i \hat{\sigma}_i^x + h_z \sum_i \hat{\sigma}_i^z\ . \tag{2.9}$$

The system parameters are $(h_x, h_z) = (1.05, 0.5)$ [50]. This model is far from integrable due to the large longitudinal field. The reduced density matrix of the initial direct product state will eventually thermalize under the time evolution generated by the time-independent Hamiltonian (2.9), the total energy always being conserved. We choose the initial states to be random product states with Hamiltonian expectation values E within a small energy interval $E \in [-0.1, 0.1]$ (close to the middle of the spectrum of $\hat{H}$), and study the spectral correlations and the emergence of a "ramp" in the spectrum of eigenvalues of the reduced density matrix at a sufficiently long time $t = 100$, when the system is fully thermalized. The results are presented in Fig. 3. We see that the spectral form factor $g(\tau) = \langle Z(\tau)Z^*(\tau)\rangle$ is indistinguishable from that computed for the "random pure state," as well as from that computed for the Floquet model, for times τ ranging from close to two orders of magnitude below the Heisenberg time scale all the way up to the plateau and it exhibits a linear "ramp" in that range of times τ. On the other hand, there is some difference in the *connected* spectral form factor $g_c(\tau) = [\langle Z(\tau)Z^*(\tau)\rangle - \langle Z(\tau)\rangle\langle Z^*(\tau)\rangle]$ displayed in Fig. 3(b): The length of the "ramp" for the Ising model is shorter than that for "random pure state," and that for the Floquet model, and shows an overshoot at early τ. This suggests that for the Ising model, whose time evolution is constrained by the energy conservation law, the subsystem is "less chaotic" in the sense that model-dependent features appear in the connected spectral form factor already at (small) times, here $\tau \approx \tau_0 = 10^4 \approx 10^{-2}\tau_H$, see Fig. 3(b), reflecting deviations from universal spectral correlations for eigenvalues λ_i at correspondingly large separations. We will discuss this issue in more detail in the next section.

III. THE DEVELOPMENT OF CHAOS AND THERMALIZATION IN FLOQUET AND ISING MODEL

In this section, we study the *development of quantum chaos* in the many-body wave function. Starting (as before) with an initial product state $|\Psi_0\rangle$, the time-evolved reduced density matrix $\hat{\rho}_A(t)$ of the subsystem,

$$\hat{\rho}_A(t) = \mathrm{Tr}_B[\hat{U}(t)|\Psi_0\rangle\langle\Psi_0|\hat{U}^\dagger(t)], \tag{3.1}$$

will eventually thermalize under the unitary time evolution operator $\hat{U}(t)$ of a generic nonintegrable system, and its spectrum will in the process develop universal spectral correlations, manifested by a linear "ramp" in the corresponding spectral form factor. In this section we ask: At what times t, under the quantum mechanical time evolution, does the "ramp" emerge, and how does it evolve in time t until it reaches its final fully thermalized regime at long times? That is, we will be studying the development of chaos in the density matrix. To answer these questions, we will study the spectral form factor at different times t before $\hat{\rho}_A(t)$ has fully thermalized.

A. Floquet system

We first study the Floquet system defined in (2.6) and (2.7) [6,46–49]. As shown in the inset of Fig. 5(b), when the subsystem size is $L_A = 9$ (total system size $L = 20$), the EE grows linearly with time $t = nT$ for time steps $n \leqslant 10$, and then quickly saturates exponentially in the time step n to the Page value. As is clearly seen from the inset of Fig. 5(b), at time step $n = 30$ the deviation of the EE from its Page value is negligible.

When we consider the *spectral form factor* $g(\tau) = \langle Z(\tau)Z^*(\tau)\rangle$ for the same density matrix $\hat{\rho}_A(t = nT)$, the "ramp" starts to emerge at time step $n = 11$: In Fig. 5(a), we can clearly observe that as the time step n increases beyond $n = 11$, the dip in $g(\tau)$ becomes much deeper, and at the same time the "ramp" is getting longer. At time step $n = 15$, the length of the "ramp" in $g(\tau) = \langle Z(\tau)Z^*(\tau)\rangle$ is already very close to that observed at time step $n = 30$. In Fig. 5(b) we plot the connected spectral form factor $g_c(\tau) = \langle Z(\tau)Z^*(\tau)\rangle - \langle Z(\tau)\rangle\langle Z^*(\tau)\rangle$, which is seen to exhibit a "ramp" whose length continues to increase beyond time step $n = 15$ until the fully thermalized regime at time step $n = 30$ is reached. These plots also show an overshoot at the low-τ end of the "ramp" in $g_c(\tau)$, which is

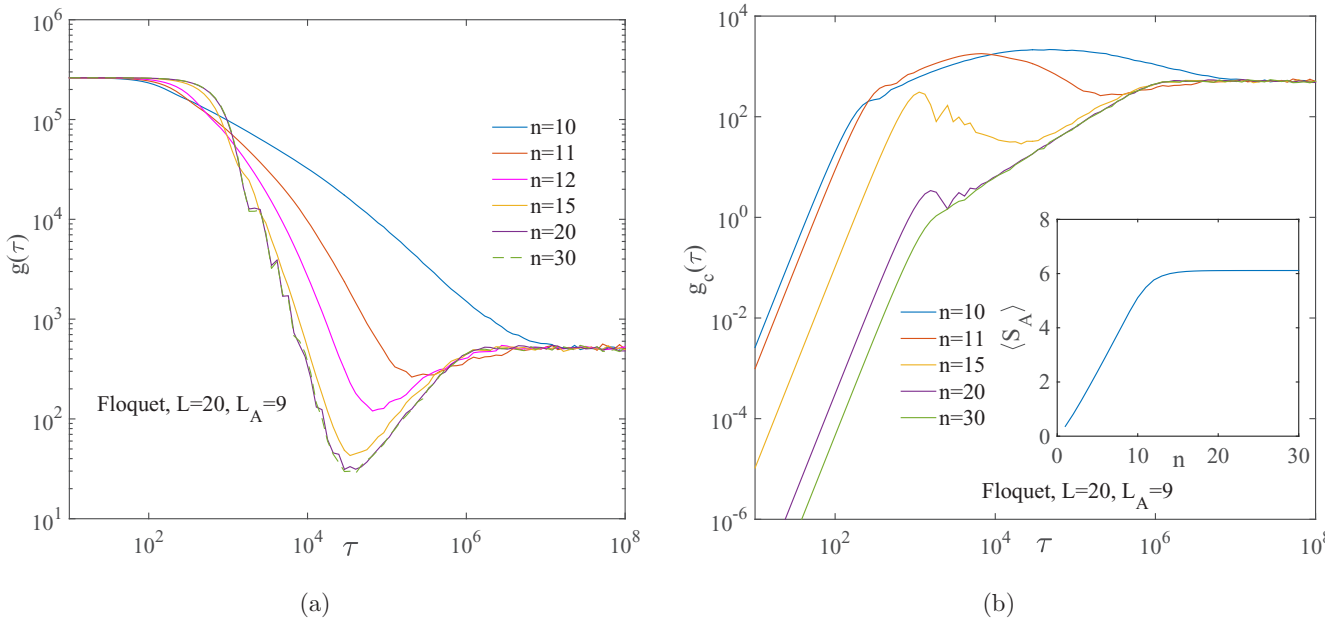

FIG. 5. (a) $g(\tau) = \langle ZZ^* \rangle$ versus τ for the Floquet model defined in (2.7) at different time steps n, averaged over 1000 samples. (b) $g_c(\tau) = \langle ZZ^* \rangle - \langle Z \rangle \langle Z^* \rangle$ for the same model at different time steps n. The inset shows the averaged entanglement entropy (EE) as a function of time step n.

however suppressed as the time step n increases further, and at $n = 30$ the overshoot has basically disappeared [and $g_c(\tau)$ is the same as that for the "random pure state"—compare Fig. 3 (b)], indicating that at this time step chaos has fully developed in the subsystem. All these time scales depend on the length L_A of the subsystem and become smaller as the subsystem size L_A is decreased.

We note that we have obtained the above results upon computing the spectral form factor by using in (1.3) or (2.2) *all* the eigenvalues of the reduced density matrix $\hat{\rho}_A(t = nT)$. Actually, in order to gain additional insight, it is useful to limit the eigenvalues used to compute the spectral form factor in (1.3) or (2.2) to a subset lying in a window around a fixed eigenvalue, and to compute the spectral form factor by only using the eigenvalues of the density matrix in this window. This procedure can then detect "local universal spectral correlations" characterizing the correlations amongst the eigenvalues in this window. In Fig. 6(a), we present results for the spectral form factor $g(\tau) = \langle Z(\tau)Z^*(\tau) \rangle$ for a window of 10 consecutive eigenvalues at the top of spectrum [51] in $\hat{\rho}_A$. We notice the appearance of a linear "ramp" as early as at time step $n = 5$. As we move the window of eigenvalues away from the top to the bottom of the spectrum of the density matrix [52], we find that the linear "ramp" develops only at later time steps—here at $n = 11$ [Fig. 6(c)]. This result demonstrates that in the Floquet model, as time t evolves, the universal spectral correlations first emerge at the top of spectrum of $\hat{\rho}_A(t = nT)$ and subsequently spread over the entire spectrum at later times t. This behavior, i.e., the fact that not the entire spectrum of the density matrix develops the spectral correlations uniformly in time t, is also responsible for the shallowness of the dip that appears, when the time step n is between 11 and 15, in the plot in Fig. 5(a) of the spectral form factor $g(\tau) = \langle Z(\tau)Z^*(\tau) \rangle$ which uses the entire spectrum as input.

Finally, we would like to discuss the connection between the linear growth of the EE and the development of universal spectral correlations. When we look at the magnitudes of the eigenvalues of $\rho_A(t)$ at early times, we find that there are only a few of them which are appreciably different from zero, and it is them that exhibit the spectral correlations and are also responsible for the observed value of the EE. Actually, they also give rise to the volume law in the EE for smaller subsystem sizes.

As time evolves, more and more eigenvalues become appreciably different from zero. They develop spectral correlations and lead to the linear growth of the EE. This is in contrast with an integrable system, where the linear growth of the EE is due to the ballistic propagation of quasiparticles [31] and there are no spectral correlations between the eigenvalues and hence there is no "ramp" in the spectral form factor [53]. In Sec. III C we will show an example of such a phenomenon within a Floquet system.

B. Ising model

In this section we investigate the development of chaos in a quantum Ising model, where the thermalization process is slower due to the presence of the energy conservation law.

High energy states: For an ensemble of initial random direct product states $|\Psi_0\rangle$ with Hamiltonian expectation value in the small energy interval $E \in [-0.1, 0.1]$ [i.e., $E = \langle \Psi_0 | \hat{H} | \Psi_0 \rangle$ in the middle of the spectrum of the Ising Hamiltonian $\hat{H}$ in (2.9)], the EE grows linearly with time until $t \approx 7$ and then saturates exponentially to the final volume law at longer times around $t = 100$ [see inset in Fig. 7(b)]. Since this initial state has energy E close to zero (middle of the spectrum of $\hat{H}$), the effective temperature is high and the saturation value of the EE is only slightly smaller than the Page value. In particular, when $L_A = 9$ (total system size $L = 20$), the difference between the

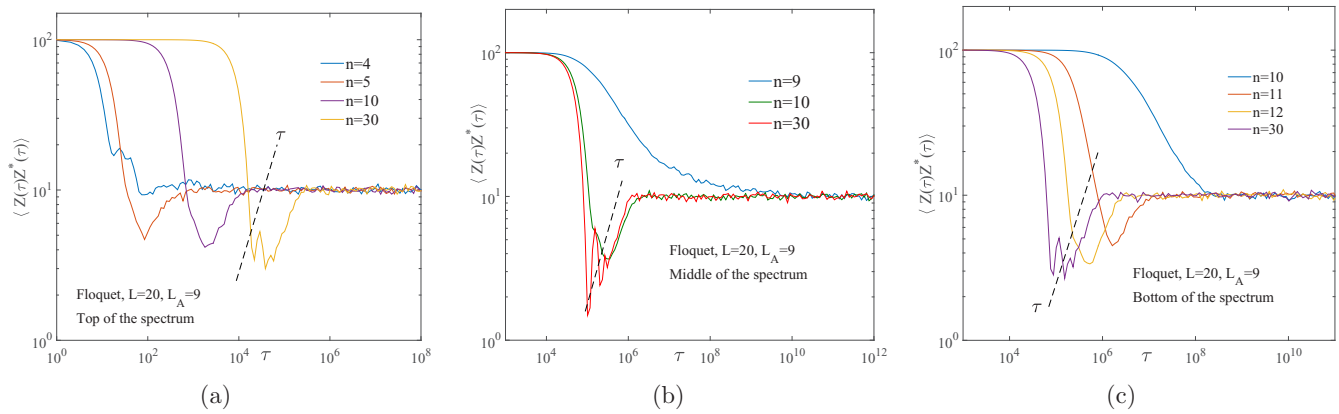

FIG. 6. (a) $g(\tau) = \langle ZZ^* \rangle$ versus τ for a subset (window) of 10 eigenvalues at the top of the spectrum of $\hat{\rho}_A$ for the Floquet model defined in (2.7) at different time steps, averaged over 1000 samples. (b) $g(\tau) = \langle ZZ^* \rangle$ for a subset of 10 eigenvalues in the middle of the spectrum of the same model. (c) $g(\tau) = \langle ZZ^* \rangle$ for a subset of 10 eigenvalues at the lower edge of the spectrum of the same model.

two values of the EE is seen to be around 0.0045, which is less than 0.1% of the EE of the Page state.

In Fig. 7, we present results for the spectral form factors $g(\tau)=\langle Z(\tau)Z^*(\tau)\rangle$ and $g_c(\tau)=\langle Z(\tau)Z^*(\tau)\rangle-\langle Z(\tau)\rangle\langle Z^*(\tau)\rangle$ at different times t. In Fig. 7(a), the "ramp" in $g(\tau)$ starts to emerge at around $t = 9$. As t increases further, the dip becomes deeper and shifts to earlier times. At $t = 15$, a linear "ramp" has fully developed and remains almost unchanged until the system is fully thermalized at $t = 100$. In Fig. 7(b) we plot the connected spectral form factor $g_c(\tau)$, which is seen to exhibit a "ramp" that continues to grow further in length, even beyond time $t = 15$. However, in contrast to the Floquet model, the overshoot appearing at the low-τ end of the "ramp" cannot be fully suppressed and is always present even after a very long time evolution [compare also Fig. 3(b)]. This indicates that the energy conservation law makes the Ising model "less chaotic" than the Floquet model, in the sense that universal spectral correlations do not extend to pairs of eigenvalues λ_i as far separated as in the Floquet model. We have also computed the spectral form factor using only a subset of eigenvalues of $\hat{\rho}_A(t)$ in a window around an eigenvalue at the top, in the middle and at the bottom of its spectrum and we find similar behavior as in the Floquet model: Universal spectral correlations first emerge at the top of the spectrum and then spread over the rest of spectrum.

Lower energy states: Since for the Ising model energy is conserved, we can also study the spectral correlations of $\hat{\rho}_A(t)$ which arise upon time evolution starting from an initial state with a lower energy E (= Hamiltonian expectation value = $\langle\psi_0|\hat{H}|\psi_0\rangle$) corresponding to properties of the quantum Ising Hamiltonian (2.9) at relatively low temperatures. (Though E is separated from the ground state by many levels, the spectrum

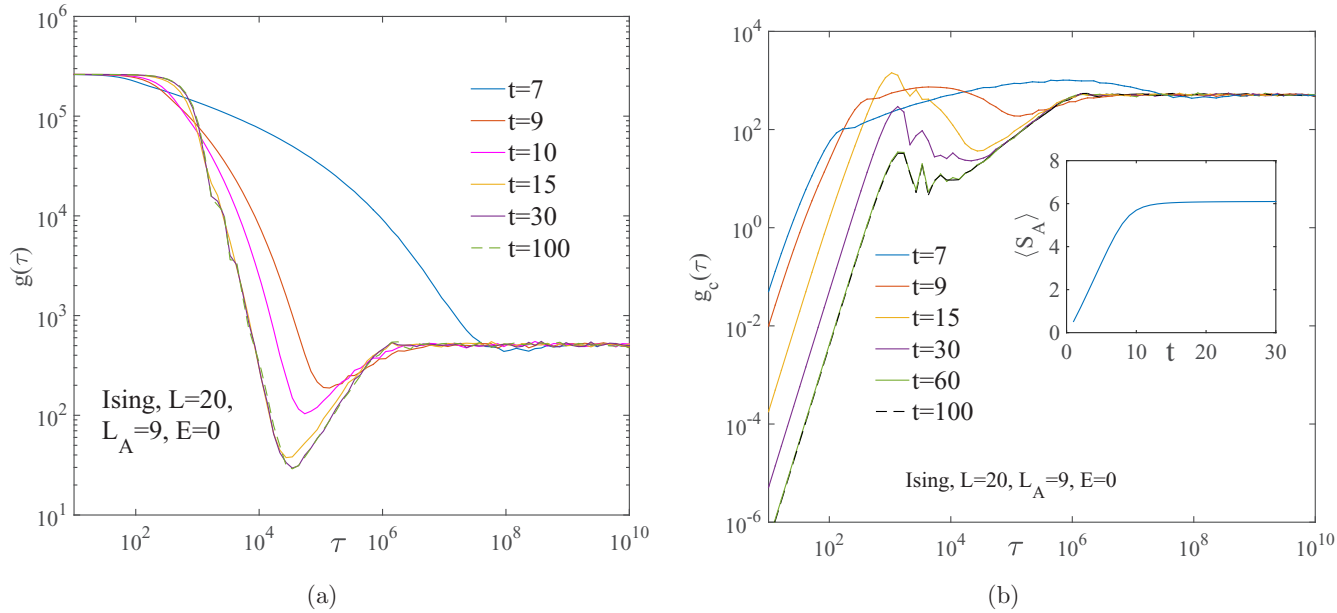

FIG. 7. (a) $g(\tau) = \langle Z(\tau)Z^*(\tau)\rangle$ versus τ of the spectrum of $\hat{\rho}_A$ for states at "high energy" expectation values $E \in [-0.1, +0.1]$ of the quantum Hamiltonian defined in (2.9), which has support in the interval $[-26, +33]$. Different curves correspond to different times t, and averages were taken over 1000 samples. (b) $g_c(\tau) = \langle Z(\tau)Z^*(\tau)\rangle - \langle Z(\tau)\rangle\langle Z^*(\tau)\rangle$ for the same model at different times t, under otherwise identical conditions. The inset shows the averaged entanglement entropy (EE) as a function of time t.

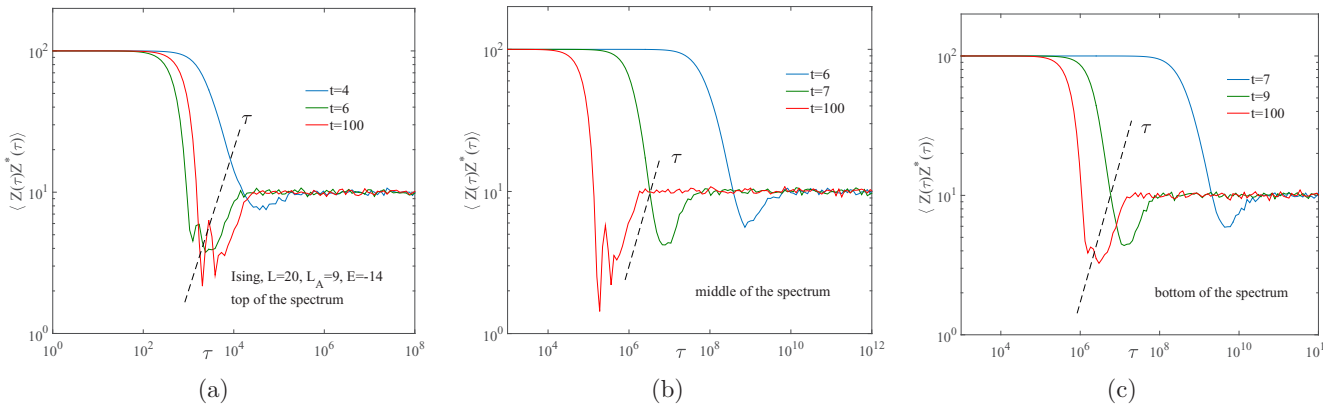

FIG. 8. (a) $g(\tau) = \langle ZZ^* \rangle$ versus τ for a subset (window) of 10 eigenvalues close to the upper edge of the spectrum of $\hat{\rho}_A$ of the quantum Ising model for states at "low energy" expectation values $E \in [-14.1, -13.9]$ of the Hamiltonian defined in (2.9), which has support in the interval $[-26, +33]$. Different curves correspond to different times t, and averages were taken over 1000 samples. (b) $g(\tau) = \langle ZZ^* \rangle$ for a subset of 10 eigenvalues in the middle of the spectrum of the same model and otherwise identical conditions. (c) $g(\tau) = \langle ZZ^* \rangle$ for a subset of 10 eigenvalues close to the lower edge of the spectrum of the same model and otherwise identical conditions.

of $\hat{H}$ has support in an interval which is approximately $[-26, +33]$.) In particular, we consider an initial direct product state close to the Neel state with an energy in the narrow interval $E \in [-14.1, -13.9]$ rather than the random product state in the middle of the spectrum of $\hat{H}$, which has high excitation energy E, considered above. Furthermore, we introduce some randomness into this ensemble of initial states so that we can perform a disorder (ensemble) average over them. Under the unitary time evolution, the EE is found to initially grow linearly with time t and to saturate as expected to a smaller volume law after long time evolution as compared to the case of a random initial state with energy E in the middle of the spectrum of $\hat{H}$. For $L_A = 9$ (total system size $L = 20$), we start to observe a dip in the spectral form factor $g(\tau) = \langle Z(\tau)Z^*(\tau) \rangle$ at times around $t = 9$. As before, we also compute the spectral form factor $g(\tau) = \langle ZZ^* \rangle$ by only using a subset of eigenvalues of $\hat{\rho}_A(t)$ locally in a window around a fixed eigenvalue of the density matrix. For a window of 10 consecutive eigenvalues close to the top of the spectrum of the density matrix $\hat{\rho}_A$ we find, similar to the Floquet model, a "ramp" already at an early time $t = 4$ which becomes linear at $t = 6$ [Fig. 8(a)]. On the other hand, as we move the window of 10 consecutive eigenvalues close to the bottom of the spectrum of the density matrix [Fig. 8(c)], the spectral correlations emerge only at later times t as compared to the case where the window is at the top of the spectrum. This is analogous to what was observed in the Floquet case.

Finally, we turn off the longitudinal field h_z in the quantum Ising Hamiltonian (2.9), so that the model becomes integrable. An initial random direct product state equilibrates after the quantum quench to a thermal state described by the generalized Gibbs ensemble (GGE) with an extensive number of conserved quantities [29–31]. As shown in Fig. 9, we do not observe any "ramp" in the spectral form factor $g(\tau) = \langle Z(\tau)Z^*(\tau) \rangle$, indicating the absence of chaos reflected in the absence of universal spectral correlations in the reduced density matrix $\hat{\rho}_A$.

C. Floquet system with prethermal regime

As discussed before, for a generic Floquet system the reduced density matrix of a general short-range entangled initial state will reach a steady state at infinite temperature after a sufficiently long time evolution, since energy is not conserved [6,46,48,54]. How thermal equilibrium and chaos emerge in the wave function is model dependent. Recently, it has been shown that a rapidly driven system may exhibit an intermediate prethermal regime of long duration in which the system reaches a thermal equilibrium state governed by an approximate time-independent Hamiltonian with the effective temperature set by the initial energy [33–36,55]. This regime can have an exponentially long lifetime (in units of inverse frequency, and other parameters of the system). We note that a prethermalized regime in a system with a time-independent (as opposed to

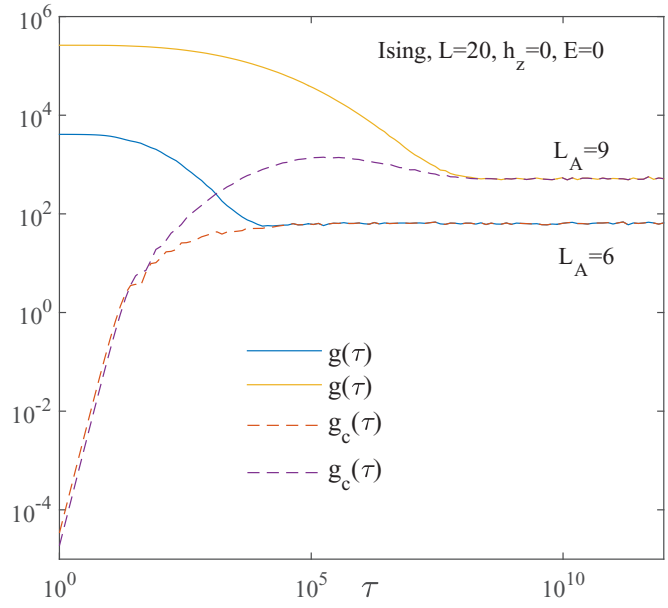

FIG. 9. $g(\tau)$ (solid curves) and $g_c(\tau)$ (dashed curves) versus τ for the quantum Ising model defined in Eq.(2.9) for the integrable case where the longitudinal field vanishes, $h_z = 0$, averaged over 1000 samples of initial random direct product states with energy expectation values in the interval $E \in [-0.1, +0.1]$, i.e., E is close to zero.

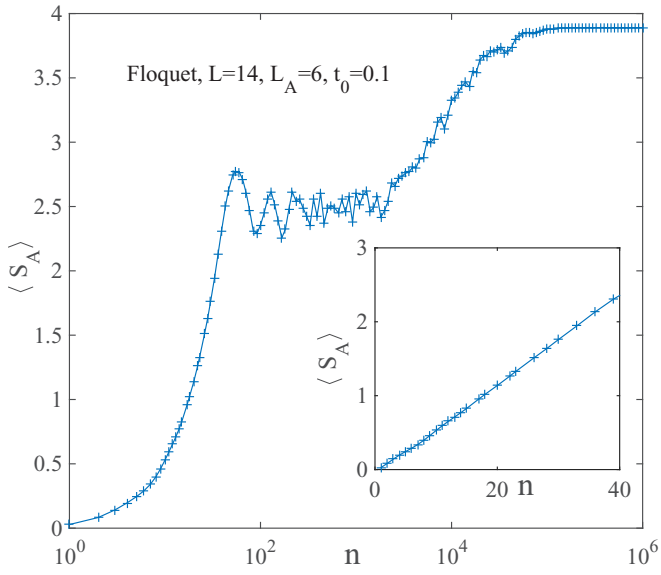

FIG. 10. Time dependence of the entanglement entropy of the Floquet system described by (3.3) on a semilog scale. The period of $T = 2t_0 = 0.2$. The result is averaged over an ensemble of 400 wave functions. The inset shows the entanglement entropy at early times on the linear scale, exhibiting linear growth as expected.

Floquet) Hamiltonian has also been considered recently in the context of nonintegrable perturbations of integrable many-body systems [56], but we do not discuss these situations here.

In this section, we are going to explore a Floquet model that exhibits such prethermalization to a thermal state which is close to that of a nearly-integrable system. The Floquet operator that we use to achieve such a prethermalized regime takes the following form,

$$\hat{U}_F = \exp[-it_0\hat{H}_1]\exp[-it_0\hat{H}_2]\,, \tag{3.2}$$

where

$$\hat{H}_1 = -\sum_{j=1}^{L-1}\hat{\sigma}_j^z\hat{\sigma}_{j+1}^z - h_x\sum_{j=1}^{L}\hat{\sigma}_j^x$$

$$\hat{H}_2 = -h_y\sum_{j=1}^{L}\hat{\sigma}_j^y\,. \tag{3.3}$$

This model is a one-dimensional periodically driven system with period $T = 2t_0$. In the numerical calculations, we choose open boundary conditions and system parameters $(h_x, h_y) = (1, 1)$. The period $T = 0.2$ is chosen to be very small in order to realize a long prethermal regime.

Since the period T is very small, it takes a large number of time steps for the Floquet system to relax to its ultimate, fully thermalized (chaotic) state. The previous method used above for rapidly thermalizing Floquet systems that simply amounted to applying the time-evolution operator many times to an initial state, which did not require diagonalizing the Floquet operator, is no longer useful here due to the large number of required time steps. Here we will instead consider a smaller system size with $L = 14$ so that we can diagonalize the Floquet operator explicitly and study the long time dynamics by applying that operator for any length of time to the initial state. We start with a random direct product state and evolve it under the Floquet operator. The result for the time evolution of the EE is shown in Fig. 10, where we clearly observe a long intermediate plateau which corresponds to the prethermalized regime. We further have computed the spectral form factor $g(\tau) = \langle Z(\tau)Z^*(\tau)\rangle$ in this (prethermalized) regime and we do not observe any dip or "ramp," demonstrating that the eigenvalues of the reduced density matrix $\hat{\rho}_A(t = nT)$ do not exhibit any universal spectral correlations in this regime. The lack of the spectral correlations shows that chaos is absent in this regime, and we expect that it is described by a generalized

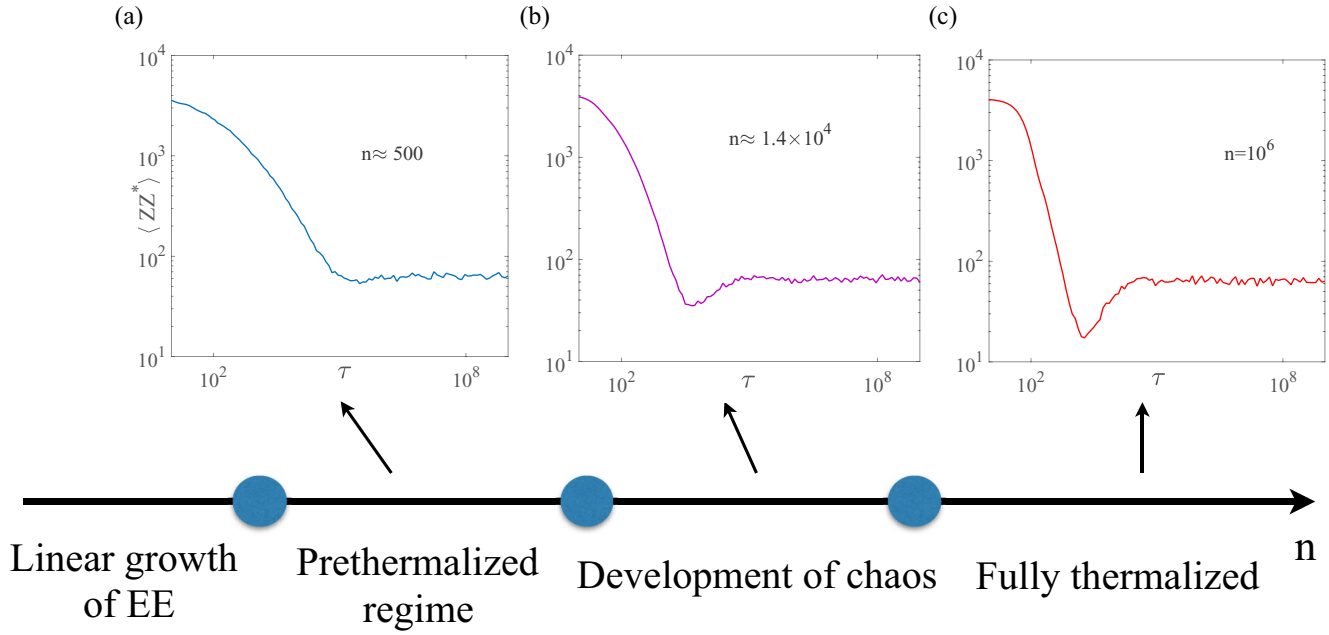

FIG. 11. Spectral form factor $g(\tau) = \langle ZZ^*\rangle$ for the Floquet model in (3.3) at different stages in the time evolution (time step n). Each curve represents the average over an ensemble of 400 wave functions.

Gibbs ensemble (GGE). On the other hand, chaos starts to appear at yet longer times where the EE increases further and eventually relaxes to the Page value; at those longer times, a small "ramp" is seen to develop in the spectral form factor depicted in Fig. 11(b). A more pronounced linear "ramp" can be observed (see Fig. 11) once the state reaches full thermalization at still larger time steps n.

Therefore, in the present Floquet model, we can separate the long time evolution into four stages (see Figs. 10 and 11): (1) a regime of linear growth of the EE, which also appears in all of the previous models (see inset of Fig. 10), (2) the prethermal regime described by GGE and absence of chaos, which is reflected by a plateau in the time evolution of the EE, (3) the regime of development of chaos where universal spectral correlations start to develop at the top of the spectrum of the density matrix $\hat{\rho}_A$, and (4) the fully thermalized regime, where the initial state has time evolved into a state whose reduced density matrix exhibits a spectrum indistinguishable from that of the density matrix of a featureless "random pure state."

IV. ANALYTICAL CALCULATIONS FOR THE "RANDOM PURE STATE"

A. Random pure state and Wishart-Laguerre ensemble

In this subsection we briefly review the connection between the reduced density matrix of the "random pure state" (Page state) and the Wishart random matrix ensemble. First, we decompose the total Hilbert space into a tensor product of the Hilbert spaces of the two subsystems A and B with dimensions N_A and N_B, respectively (assuming $N_A \leqslant N_B$ without loss of generality), and write the "random pure state" defined in (1.5) in a direct (tensor) product basis

$$|\Psi\rangle = \sum_{i=1}^{N_A}\sum_{J=1}^{N_B} X_{iJ}\,\left|\Psi_A^i\right\rangle \otimes \left|\Psi_B^J\right\rangle, \tag{4.1}$$

where the coefficients X_{iJ} are complex Gaussian random variables and form a rectangular $N_A \times N_B$ random matrix X subject to the normalization constraint $\mathrm{Tr}(XX^\dagger) = 1$. After tracing out subsystem B, we obtain from this wave function the reduced density matrix $\hat{\rho}_A = XX^\dagger$ for subsystem A, which is a $N_A \times N_A$ square matrix.

In order to make contact with the Wishart-Laguerre random matrix ensemble, we consider a (unconstrained) $N_A \times N_B$ complex random matrix $Y = \{Y_{iJ}\}$ whose statistically independent complex matrix elements are drawn from a Gaussian probability distribution

$$P(\{Y_{iJ}\}) = \mathcal{N}^{-1} \exp\left\{-\frac{\beta}{2}\, N_B \mathrm{Tr}(YY^\dagger)\right\}. \tag{4.2}$$

The $N_A \times N_A$ matrix $W \equiv YY^\dagger$ is then a random matrix belonging to what is known as the $\beta = 2$ ("GUE-type") Wishart random matrix ensemble. Consequently, the density matrix for the "random pure state," discussed above, can be expressed in terms of the Wishart random matrix as follows

$$\hat{\rho}_A \equiv \frac{YY^\dagger}{\mathrm{Tr}(YY^\dagger)}. \tag{4.3}$$

We finally note that the denominator on the right hand side of (4.3) has expectation value

$$\langle \mathrm{Tr}(YY^\dagger)\rangle = \sum_{i=1}^{N_A}\sum_{J=1}^{N_B} \langle |Y_{iJ}|^2\rangle = \frac{(N_A N_B)}{N_B} = N_A. \tag{4.4}$$

Thus, in the limit where both N_A and N_B tend to infinity while the ratio $\alpha \equiv N_A/N_B$ remains fixed, the relative fluctuations f of the random variable $\mathrm{Tr}(YY^\dagger) = N_A(1+f)$ about its mean N_A vanish, and we can replace

$$\mathrm{Tr}(YY^\dagger) \to N_A. \tag{4.5}$$

Owing to (4.3) the eigenvalues λ_i of the reduced density matrix $\hat{\rho}_A$ are thus related in the limit of large N_A and N_B to the eigenvalues μ_i of the Wishart matrix W via

$$\lambda_i = \frac{\mu_i}{N_A}. \tag{4.6}$$

Clearly, the above-described relationship immediately extends to the other two universality classes of GOE ($\beta = 1$) and GSE ($\beta = 4$) "random pure states" and Wishart random matrix ensembles.

B. Eigenvalue statistics of the Wishart-Laguerre ensemble

Here we first briefly review some important results for the Wishart-Laguerre random matrix ensemble [24]. For more details, see Appendix B.

In general, for a Wishart matrix $W = YY^\dagger$ with Y being a $N_A \times N_B$ matrix with real ($\beta = 1$), complex ($\beta = 2$) or quaternion ($\beta = 4$) Gaussian entries drawn from the joint distribution as in (4.2), the joint probability probability distribution for the N_A eigenvalues μ_i of W is known to be [24]

$$P[\{\mu_i\}] = \tilde{\mathcal{N}}^{-1} \exp[-\beta E(\{\mu_i\})], \tag{4.7}$$

where

$$E[\{\mu_i\}] = \frac{1}{2}\sum_{i}^{N}\left[V(\mu_i) - \frac{1}{2}\log|\mu_i - \mu_j|\right], \quad \mu_i > 0,$$

and $V(\mu) = (\mu - \kappa \log \mu)$ with $\kappa = (1 + N_B - N_A) - 2/\beta$; $\tilde{\mathcal{N}}^{-1}$ is a normalization factor. The weight $E[\{\mu_i\}]$ can be thought of as the energy of a one-component Coulomb gas of charges with logarithmic interaction in an external potential $V(\mu)$.

In the limit $N_A, N_B \to \infty$, the average of the spectral density

$$\hat{\nu}(\mu) \equiv \sum_{i=1}^{N_A} \delta(\mu - \mu_i), \quad \text{satisfying} \quad \int d\mu\, \hat{\nu}(\mu) = N_A, \tag{4.8}$$

of the matrix $W = YY^\dagger$ can be calculated via the saddle point approximation and is found to be equal to the so-called Marchenko-Pastur (MP) distribution [24],

$$\bar{n}(\mu) \equiv \frac{\langle \hat{\nu}(\mu)\rangle}{N_A} = \frac{1}{2\pi\alpha\mu}\sqrt{(\mu - \alpha_-)(\alpha_+ - \mu)},$$
$$\int_{\alpha_-}^{\alpha_+} d\mu\, \bar{n}(\mu) = 1, \tag{4.9}$$

where $\alpha_- \leqslant \mu \leqslant \alpha_+$ with $\alpha_\pm = (1 \pm \sqrt{\alpha})^2$, $\alpha = N_A/N_B$ and $N = N_A N_B$. This distribution is independent of the Dyson index β. Note that μ has support in the finite interval $\alpha_- \leqslant \mu \leqslant \alpha_+$ of N_A-independent length $(\alpha_+ - \alpha_-) = 4\sqrt{\alpha}$. Since all N_A eigenvalues lie in this interval, the average level spacing is

$$\overline{(\Delta\mu)} = \frac{4\sqrt{\alpha}}{N_A} \quad \text{(average level spacing of eigenvalues } \mu_i\text{)}. \tag{4.10}$$

Consider now the spectral density of the reduced density matrix $\hat{\rho}_A$ (eigenvalues $\lambda_i = \mu_i/N_A$, and $\lambda = \mu/N_A$),

$$\hat{\nu}(\lambda) \equiv \sum_{i=1}^{N_A} \delta(\lambda - \lambda_i) = N_A\, \hat{\nu}(\mu), \quad \text{satisfying}$$
$$\int d\lambda\, \hat{\nu}(\lambda) = N_A. \tag{4.11}$$

In view of (4.3) and (4.5), valid in the limit $N_A, N_B \to \infty$ which we are currently considering, it follows from (4.9) that the averaged spectral density of the density matrix $\hat{\rho}_A$ satisfies

$$\bar{n}(\lambda) \equiv \frac{\langle \hat{\nu}(\lambda)\rangle}{N_A} = N_A\, \bar{n}(\mu) = \frac{N_A}{2\pi\alpha\lambda}\sqrt{\left(\lambda - \frac{\alpha_-}{N_A}\right)\left(\frac{\alpha_+}{N_A} - \lambda\right)}, \quad \text{(where } \lambda = \mu/N_A\text{)}. \tag{4.12}$$

It follows from (4.12) that $\bar{n}(\lambda)$ is defined on the interval $\lambda \in [\alpha_-/N_A, \alpha_+/N_A]$, satisfying $\int_{\alpha_-/N_A}^{\alpha_+/N_A} d\lambda\, \bar{n}(\lambda) = 1$ by construction. Since the N_A eigenvalues λ_i of the reduced density matrix lie in the interval $\alpha_-/N_A \leqslant \lambda_i \leqslant \alpha_+/N_A$ (which becomes small when N_A becomes large), their average level spacing is

$$\overline{(\Delta\lambda)} = \frac{4\sqrt{\alpha}}{(N_A)^2}, \quad \text{(average level spacing of eigenvalues } \lambda_i\text{)}. \tag{4.13}$$

Starting from the average spectral density $\bar{n}(\lambda)$ in (4.12), we can write the Fourier transform (2.1) of the expectation value of the eigenvalue density of the reduced density matrix $\hat{\rho}_A$ as

$$\langle Z(\tau)\rangle = \int d\lambda\, \langle \hat{\nu}(\lambda)\rangle\, e^{-i\lambda\tau} = N_A \int d\lambda\, \bar{n}(\lambda)\, e^{-i\lambda\tau}. \tag{4.14}$$

When $\alpha = N_A/N_B < 1$, the density $\bar{n}(\lambda)$ vanishes at both edges, scaling as $\sqrt{|\lambda - \alpha_a/N_A|}$ as $\lambda \to \alpha_a$ where $a = \pm$ [see (4.9) above]. These two edges $\lambda = \alpha_\pm$ dominate the expectation value $\langle Z(\tau)\rangle$ and contribute

$$|\langle Z_{\alpha_\pm}(\tau)\rangle| = \frac{1}{(1 \pm \sqrt{\alpha})^2} \frac{N_A^{\frac{5}{2}}}{2\sqrt{\pi}} \alpha^{-\frac{3}{4}} \frac{1}{\tau^{3/2}}. \tag{4.15}$$

Assuming $\alpha = N_A/N_B \ll 1$, we have

$$|\langle Z(\tau)\rangle|^2 = \frac{N_A^2 N^{3/2}}{\pi\tau^3}. \tag{4.16}$$

As mentioned, the spectral form factor factorizes at early times τ, where it thus reads $\langle Z(\tau)Z^*(\tau)\rangle \approx |\langle Z(\tau)\rangle|^2 \sim 1/\tau^3$. This is in agreement with the numerical results shown in Figs. 2 and 3.

On the other hand, when $\alpha = N_A/N_B = 1$, the lower edge for MP distribution (4.9) is pushed to $\alpha_- = 0$ and the spectral density has a $1/\lambda^{1/2}$ divergence at this edge. This divergence will lead to a different behavior of $\langle Z(\tau)\rangle$, namely

$$\langle Z(\tau)\rangle = \frac{N_A^2}{2\pi}\int_0^{4/N_A} d\lambda \sqrt{\frac{4/N_A - \lambda}{\lambda}} e^{-i\lambda\tau} = N_A\left[J_0\left(\frac{2\tau}{N_A}\right) + i\, J_1\left(\frac{2\tau}{N_A}\right)\right] e^{-\frac{2i\tau}{N_A}}, \tag{4.17}$$

where $J_\alpha(z)$ is the Bessel function of the first kind, which behaves in the limit $z \gg 1$ as $|J_\alpha(z)| \sim 1/\sqrt{2\pi z}$. This leads to

$$|\langle Z(\tau)\rangle|^2 \sim \frac{N_A^3}{\pi\tau}, \tag{4.18}$$

which decays much slower than in the case $\alpha < 1$ displayed in (4.16). This is also in agreement with the numerical results in Fig. 2 and Fig. 3.

C. Spectral form factor for the reduced density matrix from Wishart random matrix theory

For any random matrix ensemble with the joint probability density described by (4.7), the level-level correlation function ("pair correlation function") is universal and only depends [57,58] on the symmetry type, although the spectral density depends on the explicit form of the potential $V(\mu_i)$ defined in (4.7). Specifically, the connected correlation function of the spectral density $\hat{\nu}(\lambda)$, defined in (4.11), takes for Dyson index $\beta = 2$ ("GUE-type" class) in the large N_A limit the following universal form which can be expressed in terms of the celebrated so-called sine-kernel [57–59],

$$\langle \hat{\nu}(\lambda)\hat{\nu}(\lambda')\rangle - \langle \hat{\nu}(\lambda)\rangle\, \langle \hat{\nu}(\lambda')\rangle = \langle \hat{\nu}(E)\rangle \delta(\omega) - \langle \hat{\nu}(\lambda)\rangle\, \langle \hat{\nu}(\lambda')\rangle\, \frac{\sin^2[\pi\langle \hat{\nu}(E)\rangle\omega]}{[\pi\langle \hat{\nu}(E)\rangle\omega]^2}, \tag{4.19}$$

where

$$\omega = \lambda - \lambda', \quad E = (\lambda + \lambda')/2. \tag{4.20}$$

(For more details see Appendix B 3.) We also recall $\langle \hat{\nu}(\lambda)\rangle = N_A\, \bar{n}(\lambda)$ from (4.12). Here, in order to obtain a universal expression, the argument of the sine function was rescaled by the nonuniversal factor $\langle \hat{\nu}(E)\rangle$ that determines the local mean level spacing [60].

The spectral form factor

$$g(\tau) = \langle Z(\tau)Z^*(\tau)\rangle = [\langle Z(\tau)Z^*(\tau)\rangle - \langle Z(\tau)\rangle\langle Z^*(\tau)\rangle] + \langle Z(\tau)\rangle\langle Z^*(\tau)\rangle = g_c(\tau) + \langle Z(\tau)\rangle\langle Z^*(\tau)\rangle \tag{4.21}$$

is related to the level-level correction function $\langle \hat{\nu}(\lambda)\hat{\nu}(\lambda')\rangle$ through Fourier transformation,

$$g_c(\tau) = \int d\lambda d\lambda' \left[\langle \hat{\nu}(\lambda)\hat{\nu}(\lambda')\rangle - \langle \hat{\nu}(\lambda)\rangle\langle \hat{\nu}(\lambda')\rangle\right] e^{-i(\lambda-\lambda')\tau}, \tag{4.22}$$

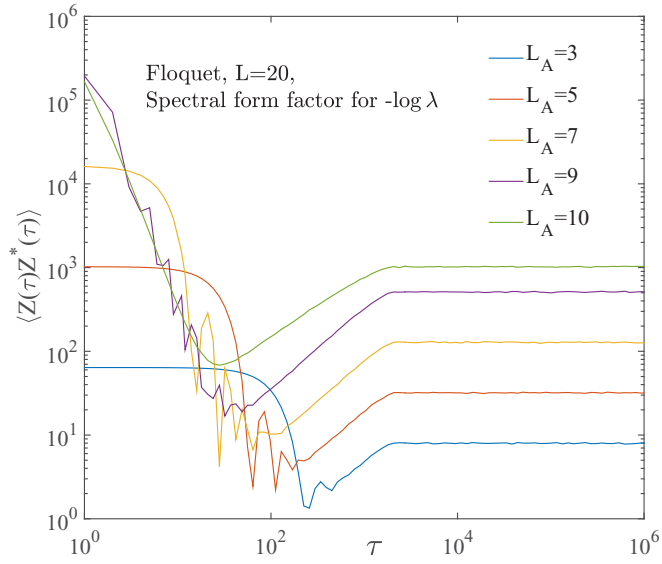

FIG. 12. Spectral form factor of the entanglement Hamiltonian.

and we focus here on the connected function $g_c(\tau)$ as the disconnected part has already been discussed in Sec. IV B. Taking the Fourier transform of the sine kernel in (4.19) which is determined by the following elementary integral (a is any real parameter)

$$\int_{-\infty}^{\infty} e^{-i\omega\tau}\,\frac{\sin^2[\pi a\omega]}{\pi^2\omega^2}d\omega = \begin{cases} a-\frac{|\tau|}{2\pi}, & |\tau|<2\pi a \\ 0, & |\tau|\geqslant 2\pi a \end{cases}, \quad (4.23)$$

we obtain (for more details see Appendix B 3)

$$g_c(\tau) = \begin{cases} \frac{2}{\pi}\frac{1}{\sqrt{N}}\,|\tau|, & |\tau|<\tau_H \\ N_A, & |\tau|>\tau_H \end{cases},$$
$$\text{where}\quad \tau_H = (2\pi/\overline{(\Delta\lambda)}) = \frac{\pi}{2}N_A\sqrt{N}, \quad (4.24)$$

where we recall that $N = N_A N_B$. The regime of linear growth with τ is universal and reflects the universal spectral correlations present in the spectrum, which are represented by the sine kernel on the right hand side of (4.19). Note also that the prefactor of the linear growth term in (4.24) is independent of subsystem size N_A. This is the origin of the fact that the linear "ramps" appearing for different subsystem sizes N_A all lie on top of each other—see, e.g., Fig. 2. The spectral form factors of the entanglement Hamiltonian, discussed in Appendix A and depicted in Fig. 12, do not show this feature but are instead shifted with respect to each other by a N_A-dependent constant (on a log-log plot), reflecting a N_A-dependent coefficient of the term linear in τ.

In view of (4.16),(4.18),(4.21),(4.24), the disconnected part in $g(\tau)$ hides the early-time τ part of the universal linear "ramp" (4.24) appearing in $g_c(\tau)$. This effect gives rise to the "dip" (minimum) in $g(\tau)$ and allows one to estimate the "dip time" τ_d as follows: Equating $|\langle Z(\tau)\rangle|^2$ and the "ramp" in (4.24) gives the dip time in $\langle Z(\tau)Z^*(\tau)\rangle$. Based on this logic, we expect the dip time τ_d to be around $(N_A N)^{1/2}$ when $\alpha<1$, which is consistent with the numerical results. On the other hand, when $\alpha=1$, this logic yields $\tau_d \sim N_A^2$. However this is a time scale of the order of the plateau time $\tau_p = \tau_H$, and therefore we cannot observe the "ramp" in $g(\tau) = \langle Z(\tau)Z^*(\tau)\rangle$ when $\alpha=1$, consistent with our numerical findings reported above.

V. DISCUSSION AND CONCLUSION

In conclusion, we have explored the presence of universal spectral correlations in the spectrum of the reduced density matrix $\hat{\rho}_A$ of a many-body wave function and used the presence of these correlations to define quantum chaos at the level of a single many-body wave function. To detect these spectral correlations, we constructed the spectral form factor $g(\tau)$ for $\hat{\rho}_A$ and identified the presence of a "ramp" as a hallmark of the spectral correlations. We explicitly considered three wave functions: the "random pure state," a typical state of a Floquet spin model, and of a quantum Ising model in both transverse and longitudinal fields, both in one spatial dimension. In all three cases, we numerically found the presence of the universal linear "ramp" in the spectral form factor. For the "random pure state," we also analytically computed the spectral form factor by using Wishart random matrix theory and found agreement with our numerical results.

Moreover, we discussed how universal spectral correlations develop in a quantum quench problem from an initial product state lacking chaos. We found that the spectral correlations first emerge at the top of spectrum of the reduced density matrix $\hat{\rho}_A$, and then spread over the entire spectrum at later times. We verified this statement numerically in both the Floquet and quantum Ising models. Finally we studied a rapidly driven Floquet system which possesses a long prethermalized regime exhibiting an "EE plateau," on which the system can be well approximated by a GGE. For times when the system is on that EE plateau, we don't observe any "ramp" in the spectral form factor, which is consistent with the absence of chaos in the GGE. We found that universal spectral correlations (and a "ramp") in the density matrix develop only when the wave function starts to relax to the fully thermalized regime at late times.

ACKNOWLEDGMENTS

We thank C. Nayak for the discussion on the prethermalized regime. X.C. was supported by a postdoctoral fellowship from the Gordon and Betty Moore Foundation, under the EPiQS initiative, Grant No. GBMF4304, at the Kavli Institute for Theoretical Physics. This work was supported by the NSF under Grant No. DMR-1309667 (AWWL). We acknowledge support from the Center for Scientific Computing from the CNSI, MRL: an NSF MRSEC (DMR-1121053).

APPENDIX A: SPECTRAL FORM FACTOR OF THE ENTANGLEMENT HAMILTONIAN

Numerical results for the spectral form factor of the entanglement Hamiltonian $\hat{H}_E$ of the "random pure state" are displayed in Fig. 12 and are to be compared with the spectral form factor of the reduced density matrix $\hat{\rho}_A$ of the same system, depicted in Fig. 2. We see that both spectral form factors exhibit a linear "ramp" (unit slope on the log-log plot),

which is the hallmark of universal spectral correlations. The form factors of the entanglement Hamiltonian are shifted by a N_A-dependent constant on the log-log plot, which reflects a N_A-dependent prefactor of the linear τ dependence. Recall that entanglement Hamiltonian and density matrix are related as in (1.4), and that, as mentioned in the sentence below (1.4), the spectral form factor of the former is obtained from that of the latter by letting $\lambda_i \to -\ln \lambda_i$, where λ_i denotes the eigenvalues of the reduced density matrix.

APPENDIX B: SOME DETAILS ON WISHART RANDOM MATRIX THEORY

1. Unscaled Gaussian Probability Weight

In general, for a Wishart matrix $\mathcal{W} = YY^\dagger$ with Y being an arbitrary $N_A \times N_B$ matrix with real ($\beta=1$), complex ($\beta=2$), or quaternion ($\beta = 4$) Gaussian entries drawn from the probability distribution

$$\mathcal{P}(\{Y_{iJ}\}) = \mathcal{N}^{-1} \exp\left\{-\frac{\beta}{2}\mathrm{Tr}(YY^\dagger)\right\}, \tag{B1}$$

the joint probability distribution for the N_A eigenvalues ξ_i of $\mathcal{W}$ is known to be [24]

$$\mathcal{P}[\{\xi_i\}] = C_{N_A,N_B} e^{-\frac{\beta}{2}\sum_{i=1}^{N_A}\xi_i} \prod_{i=1}^{N_A} \xi_i^{\kappa\beta/2} \times \prod_{1\leqslant j<k\leqslant N_A} |\xi_j - \xi_k|^\beta, \quad \xi_i > 0, \tag{B2}$$

where $\kappa = (1 + N_B - N_A) - 2/\beta$ and C_{N_A,N_B} is a normalization factor. This expression can be written in standard Boltzmann form, $\mathcal{P}[\{\xi_i\}] \propto \exp[-\beta E(\{\xi_i\})]$, where

$$E[\{\xi_i\}] = \frac{1}{2}\sum_i^N \left[V(\xi_i) - \frac{1}{2}\log|\xi_i - \xi_j|\right] \tag{B3}$$

can be thought of as the energy of a one-component Coulomb gas of charges with logarithmic interaction in an external potential

$$V(\xi) = (\xi - \kappa \log \xi). \tag{B4}$$

In the limit $N_A, N_B \to \infty$ with $\alpha = N_A/N_B =$ fixed, the spectral density can be computed via the saddle point approximation leading to the Marchenko-Pastur (MP) distribution

$$\bar{n}(\xi) \equiv \frac{\langle\hat{\nu}(\xi)\rangle}{N_A} = \lim_{N_A,N_B\to\infty}\left\langle \frac{1}{N_A}\sum_i \delta(\xi - \xi_i)\right\rangle = \frac{1}{2\pi\alpha\xi}\sqrt{\left(\frac{\xi}{N_B} - \alpha_-\right)\left(\alpha_+ - \frac{\xi}{N_B}\right)}, \tag{B5}$$

where $\alpha_\pm = (1 \pm \sqrt{\alpha})^2$ and $N_B\alpha_- \leqslant \xi \leqslant N_B\alpha_+$. This distribution is independent of the Dyson index β and by construction satisfies $\int_{N_B\alpha_-}^{N_B\alpha_+} d\xi\ \bar{n}(\xi) = 1$.

2. Scaled Gaussian—N_A-independent Spectral Density

It is convenient to rescale the Wishart random matrix and consequently also its eigenvalues

$$\mathcal{W} \equiv N_B\, W, \quad W = YY^\dagger, \quad \xi_i \equiv N_B\, \mu_i \tag{B6}$$

so that

$$P(\{Y_{iJ}\}) = \tilde{\mathcal{N}}^{-1} \exp\left\{-\frac{\beta}{2}N_B\ \mathrm{Tr}(YY^\dagger)\right\}. \tag{B7}$$

We can think of this as rescaling $\beta \to \beta\ N_B$. Now, the joint probability distribution for the N_A eigenvalues μ_i of the Wishart matrix W can be written in standard Boltzmann form, $P[\{\mu_i\}] \propto \exp[-\beta N_B E(\{\mu_i\})]$, with $E[\{\mu_i\}]$ the same function as in (4.7). In the limit $N_A, N_B \to \infty$, we obtain from (B5) the spectral distribution [noting that $\bar{n}(\xi)\, d\xi = \bar{n}(\mu)\, d\mu$]

$$\bar{n}(\mu) = \lim_{N_A,N_B\to\infty}\frac{\langle\hat{\nu}(\mu)\rangle}{N_A} = \frac{1}{2\pi\alpha\mu}\sqrt{(\mu - \alpha_-)(\alpha_+ - \mu)}. \tag{B8}$$

In this form the distribution becomes *independent* of N_A, N_B in the limit when these are large, and the result depends only on $\alpha = N_A/N_B$ which we consider holding fixed.

As already discussed in the paragraph surrounding (4.4), we have the expectation value

$$\langle \mathrm{Tr}(YY^\dagger)\rangle = \sum_{i=1}^{N_A}\sum_{J=1}^{N_B}\langle|Y_{iJ}|^2\rangle = \frac{(N_A N_B)}{N_B} = N_A. \tag{B9}$$

Thus, in the limit where both N_A and N_B tend to infinity while the ratio $\alpha \equiv N_A/N_B$ remains fixed, we can replace

$$\mathrm{Tr}(YY^\dagger) \to N_A \tag{B10}$$

in the usual sense. We see from ((B6), (B7)) that the eigenvalues λ_i of the reduced density matrix $\hat{\rho}_A$ are related in the limit of large N_A and N_B to the eigenvalues μ_i of the Wishart matrix W via

$$\lambda_i = \frac{\mu_i}{N_A}. \tag{B11}$$

3. Some details about the computation of the Spectral Form Factor for the ("GUE-type"-) Wishart Random Matrix Ensemble in (4.24)

We can express the spectral form factor (1.3) as follows in terms of the density of states (4.11)

$$\begin{aligned} g(\tau) &= \left\langle \sum_{i,j} e^{-i\tau(\lambda_i - \lambda_j)}\right\rangle \\ &= \left\langle \sum_{i,j}\left[\int d\lambda\ \delta(\lambda - \lambda_i)\right] \times \left[\int d\lambda'\ \delta(\lambda' - \lambda_j)\right] e^{-i\tau(\lambda_i - \lambda_j)}\right\rangle \\ &= \int d\lambda \int d\lambda'\, e^{-i\tau(\lambda - \lambda')}\left\langle \sum_{i,j}\delta(\lambda - \lambda_i)\,\delta(\lambda' - \lambda_j)\right\rangle \\ &= \int d\lambda \int d\lambda'\, e^{-i\tau(\lambda - \lambda')}\,\langle\hat{\nu}(\lambda)\,\hat{\nu}(\lambda')\rangle. \end{aligned} \tag{B12}$$

Using (4.11) we obtain from (B12)

$$g(\tau) = \int d\mu \int d\mu'\ e^{-i(\tau/N_A)(\mu - \mu')}\ \langle\hat{\nu}(\mu)\,\hat{\nu}(\mu')\rangle. \tag{B13}$$

The (2-point) correlation function of the density of states (4.11) appearing in ((B12),(B13)) above can be re-written as follows

$$\begin{aligned}\langle\hat{\nu}(\mu)\,\hat{\nu}(\mu')\rangle &= \left\langle \sum_{i,j}\,\delta(\mu-\mu_i)\,\delta(\mu'-\mu_j)\right\rangle \\ &= \left\langle \sum_{i}\,\delta(\mu-\mu_i)\,\delta(\mu'-\mu_i)\right\rangle \\ &\quad + \left\langle \sum_{i\neq j}\,\delta(\mu-\mu_i)\,\delta(\mu'-\mu_j)\right\rangle \\ &= \delta(\mu-\mu')\left\langle \sum_{i}\,\delta(\mu-\mu_i)\right\rangle \\ &\quad + \left\langle \sum_{i\neq j}\,\delta(\mu-\mu_i)\,\delta(\mu'-\mu_j)\right\rangle \\ &= \delta(\mu-\mu')\,\langle\hat{\nu}(\mu)\rangle \\ &\quad + \left\langle \sum_{i\neq j}\,\delta(\mu-\mu_i)\,\delta(\mu'-\mu_j)\right\rangle, \end{aligned} \tag{B14}$$

and thus the connected function reads

$$\begin{aligned}\langle\hat{\nu}(\mu)\,\hat{\nu}(\mu')\rangle_c &= \langle\hat{\nu}(\mu)\,\hat{\nu}(\mu')\rangle \;-\; \langle\hat{\nu}(\mu)\rangle\;\langle\hat{\nu}(\mu')\rangle \\ &= \delta(\mu-\mu')\,\langle\hat{\nu}(\mu)\rangle + \langle\hat{\nu}(\mu)\rangle\,\langle\hat{\nu}(\mu')\rangle \\ &\quad\times\left[\frac{\left\langle\sum_{i\neq j}\,\delta(\mu-\mu_i)\delta(\mu'-\mu_j)\right\rangle}{\langle\hat{\nu}(\mu)\rangle\,\langle\hat{\nu}(\mu')\rangle} - 1\right]. \end{aligned} \tag{B15}$$

Note that $\langle\sum_{i\neq j}\,\delta(\mu-\mu_i)\delta(\mu'-\mu_j)\rangle$ equals $N_A(N_A-1)$ times the probability that one eigenvalue equals μ and another eigenvalue equals $\mu'(\neq\mu)$, as computed from (4.7).

When μ and μ' are separated by much less than N_A level spacings, so that we can approximate $\langle\nu(\mu)\rangle \approx \langle\nu(\mu')\rangle \approx \langle\nu(\mathcal{E})\rangle$, where

$$\mathcal{E} \equiv \frac{\mu+\mu'}{2}, \quad \Omega \equiv (\mu-\mu'), \tag{B16}$$

the square bracket in (B15) is known analytically ("sine kernel') to be [57–59]

$$\begin{aligned}&\left[\frac{\langle\hat{\nu}(\mu)\hat{\nu}(\mu')\rangle}{\langle\hat{\nu}(\mu)\rangle\,\langle\hat{\nu}(\mu')\rangle} - 1\right] \\ &= (\text{when } \Omega=(\mu-\mu')\neq 0) \\ &= \left[\frac{\left\langle\sum_{i\neq j}\,\delta(\mu-\mu_i)\delta(\mu'-\mu_j)\right\rangle}{\langle\hat{\nu}(\mu)\rangle\,\langle\hat{\nu}(\mu')\rangle} - 1\right] \\ &= (-1)\,\frac{\sin^2[\pi\,\langle\hat{\nu}(\mathcal{E})\rangle\Omega]}{[\pi\,\langle\hat{\nu}(\mathcal{E})\rangle\Omega]^2}. \end{aligned} \tag{B17}$$

Analogous to what was mentioned in the paragraph below (4.20), the argument of the sine function is rescaled by the nonuniversal factor $\langle\hat{\nu}(\mathcal{E})\rangle$ which equals the inverse of the local mean level spacing of eigenvalues μ_i at $\mu=\mathcal{E}$.

We now provide some detailed steps for obtaining (4.24). The connected spectral form factor on the left hand side of this equation now reads explicitly

$$\begin{aligned}g_c(\tau) &= \int d\mu \int d\mu'\; e^{-i(\mu-\mu')(\tau/N_A)}\;\langle\hat{\nu}(\mu)\,\hat{\nu}(\mu')\rangle_c \\ &= \int d\mathcal{E}\int d\Omega\, e^{-i\Omega(\tau/N_A)}\Big[\langle\hat{\nu}(\mathcal{E})\rangle\;\delta(\Omega) \\ &\quad - \langle\hat{\nu}(\mathcal{E}+\Omega/2)\rangle\;\langle\hat{\nu}(\mathcal{E}-\Omega/2)\rangle\;\frac{\sin^2[\pi\,\langle\hat{\nu}(\mathcal{E})\rangle\Omega]}{[\pi\,\langle\hat{\nu}(\mathcal{E})\rangle\Omega]^2}\Big], \end{aligned} \tag{B18}$$

or

$$\begin{aligned}g_c(\tau) &= \int d\mathcal{E}\int d\Omega\, e^{-i\Omega(\tau/N_A)}\Big[\langle\hat{\nu}(\mathcal{E})\rangle\;\delta(\Omega) \\ &\quad - R(\mathcal{E},\Omega)\;\frac{\sin^2[\pi N_A\langle\hat{\nu}(\mathcal{E})\rangle\Omega]}{[\pi\Omega]^2}\Big], \end{aligned} \tag{B19}$$

where

$$R(\mathcal{E},\Omega) \equiv \frac{\langle\hat{\nu}(\mathcal{E}+\Omega/2)\rangle\;\langle\hat{\nu}(\mathcal{E}-\Omega/2)\rangle}{\langle\hat{\nu}(\mathcal{E})\rangle^2}. \tag{B20}$$

Next, we implement a version of an idea that was used in Ref. [12] for the computation of the spectral form factor of a random GUE *Hamiltonian* in the context of the SYK model. In particular, we limit the integral over Ω by introducing a cutoff Ω_0,

$$\int d\Omega \to \int_{-\Omega_0/2}^{+\Omega_0/2} d\Omega, \tag{B21}$$

chosen to satisfy the requirement that the density of states $\langle\hat{\nu}(\mathcal{E}+\Omega/2)\rangle$ does not vary appreciably when $-\Omega_0/2 < \Omega < +\Omega_0/2$. Then the factor R in the integrand in (B19) becomes unity, $R(\mathcal{E},\Omega)\to 1$. [Physically, the cutoff of course implies that variations of $g_c(\tau)$ on time scales $(\tau/N_A) \lessapprox (1/\Omega_0)$ can no longer be resolved.] Now we divide the interval $[\alpha_-,\alpha_+]$ in which all eigenvalues μ_i have support, into a set of nonoverlapping subintervals of length Ω_0 each. The integral of Ω over each subinterval number $I=1,2,\ldots,M$ at fixed $\mathcal{E}_I$ (say at the center of the interval) can now be done in the limit $N_A\to\infty$ by using (4.23) and the fact that in that limit $\langle\hat{\nu}(\mathcal{E}_I)\rangle = N_A\,\bar{n}(\mathcal{E}_I)$, where $\bar{n}(\mathcal{E}_I)$ is a N_A-independent constant [see (4.9)]:

$$\begin{aligned}&\int_{-\Omega_0/2}^{+\Omega_0/2} e^{-i\Omega(\tau/N_A)}\;\frac{\sin^2[\pi N_A\,\bar{n}(\mathcal{E}_I)\Omega]}{[\pi\Omega]^2}\;d\Omega \\ &= \frac{N_A\bar{n}(\mathcal{E}_I)}{\pi^2}\int_{-N_A\bar{n}(\mathcal{E}_I)\Omega_0/2}^{+N_A\bar{n}(\mathcal{E}_I)\Omega_0/2} e^{-i\Omega'\tau/N_A^2\bar{n}(\mathcal{E}_I)}\;\frac{\sin^2[\pi\Omega']}{[\Omega']^2}\;d\Omega' \\ &\sim \frac{N_A\bar{n}(\mathcal{E}_I)}{\pi^2}\int_{-\infty}^{+\infty} e^{-i\Omega'\tau/N_A^2\bar{n}(\mathcal{E}_I)}\;\frac{\sin^2[\pi\Omega']}{(\omega')^2}\;d\Omega' \\ &= \frac{N_A\bar{n}(\mathcal{E}_I)}{\pi^2}\begin{cases}\pi^2 - \frac{\pi}{2}\frac{|\tau|}{N_A^2\bar{n}(\mathcal{E}_I)}, & \frac{|\tau|}{N_A^2\bar{n}(\mathcal{E}_I)} < 2\pi \\ 0, & \frac{|\tau|}{N_A^2\bar{n}(\mathcal{E}_I)} > 2\pi\end{cases} \\ &= \begin{cases}N_A\bar{n}(\mathcal{E}_I) - \frac{1}{2\pi}\frac{|\tau|}{N_A}, & \frac{|\tau|}{N_A} < 2\pi N_A\bar{n}(\mathcal{E}_I) \\ 0, & \frac{|\tau|}{N_A} > 2\pi N_A\bar{n}(\mathcal{E}_I)\end{cases}. \end{aligned}$$

For subinterval number I, at fixed $\mathcal{E}_I$, we thus obtain a "ramp,"

$$g_c^{(I)}(\tau) = \begin{cases} \frac{1}{2\pi}\frac{|\tau|}{N_A}, & \frac{1}{2\pi}\frac{|\tau|}{N_A} < N_A\bar{n}(\mathcal{E}_I) \\ N_A\bar{n}(\mathcal{E}_I), & \frac{1}{2\pi}\frac{|\tau|}{N_A} > N_A\bar{n}(\mathcal{E}_I) \end{cases}$$
$$= \min\left\{\frac{1}{2\pi}\frac{|\tau|}{N_A}\ ,\ N_A\bar{n}(\mathcal{E}_I)\right\}. \tag{B22}$$

Now, doing the integral over $\mathcal{E}$ as a sum over the subintervals,

$$\int_{\alpha_-}^{\alpha_+} d\mathcal{E} \to \sum_{I=1}^{M} \Omega_0, \tag{B23}$$

where $\alpha_\pm$ were defined immediately below (4.9), we obtain from (B22)

$$g_c(\tau) = \sum_{i=1}^{M} \Omega_0\ g_c^{(I)}(\tau)$$
$$= \min\left\{\int_{\alpha_-}^{\alpha_+} d\mathcal{E}\ \frac{1}{2\pi}\frac{|\tau|}{N_A}\ ,\ \int_{\alpha_-}^{\alpha_+} d\mathcal{E}\ N_A\ \bar{n}(\mathcal{E})\right\}$$
$$= \min\left\{\left(\frac{\alpha_+ - \alpha_-}{N_A}\right)\frac{|\tau|}{2\pi},\ N_A\right\} = \min\left\{\frac{2\sqrt{\alpha}|\tau|}{\pi N_A},\ N_A\right\}, \tag{B24}$$

where we used $(\alpha_+ - \alpha_-)/N_A = \frac{4\sqrt{\alpha}}{N_A} = \frac{4}{\sqrt{N}}$, recalling $\alpha = N_A/N_B$, as well as the normalization of $\bar{n}(\mu)$ from (4.9). We now obtain (4.24) from (B24), since $\frac{4}{\sqrt{N}}\frac{|\tau_H|}{2\pi} = N_A$ leads to $\tau_H = \frac{\pi}{2}N_A\sqrt{N}$. The Heisenberg time is defined to be 2π times the inverse of the mean level spacing (here of the reduced density matrix $\hat{\rho}_A$), and this yields (setting $\hbar = 1$) upon using (4.13) $\tau_H = (2\pi/\overline{(\Delta\lambda)}) = \frac{\pi}{2}(N_A^2/\sqrt{\alpha}) = \frac{\pi}{2}N_A\sqrt{N}$ in agreement with the above result. In conclusion we have obtained the following result for the connected spectral form factor,

$$g_c(\tau) = N_A \begin{cases} \frac{|\tau|}{\tau_H}, & |\tau| < \tau_H \\ 1, & |\tau| > \tau_H \end{cases},$$
$$\text{where}\quad \tau_H = (2\pi/\overline{(\Delta\lambda)}) = \frac{\pi}{2}N_A\sqrt{N} \tag{B25}$$
$$= \begin{cases} \frac{2}{\pi}\frac{1}{\sqrt{N}}|\tau|, & |\tau| < \tau_H \\ N_A, & |\tau| > \tau_H \end{cases},$$
$$\text{where}\quad \tau_H = (2\pi/\overline{(\Delta\lambda)}) = \frac{\pi}{2}N_A\sqrt{N}. \tag{B26}$$

The last equation, displaying explicitly the N_A independence of the prefactor of the linear growth in τ, is the result shown in (4.24).

[1] M. Srednicki, Phys. Rev. E **50**, 888 (1994).
[2] J. M. Deutsch, Phys. Rev. A **43**, 2046 (1991).
[3] F. Haake, *Quantum Signatures of Chaos* (Springer Science & Business Media, Berlin, 2013), Vol. 54.
[4] H. Stoeckmann, *Quantum Chaos, An Introduction* (Cambridge University Press, New York, 1999).
[5] T. Guhr, A. Müller-Groeling, and H. A. Weidenmüller, Phys. Rep. **299**, 189 (1998).
[6] L. D'Alessio and M. Rigol, Phys. Rev. X **4**, 041048 (2014).
[7] S. H. Shenker and D. Stanford, J. High Energy Phys. 12 (2014) 46.
[8] S. H. Shenker and D. Stanford, J. High Energy Phys. 3 (2014) 67.
[9] S. H. Shenker and D. Stanford, J. High Energy Phys. 5 (2015) 132.
[10] J. Maldacena, S. H. Shenker, and D. Stanford, J. High Energy Phys. 8 (2016) 106.
[11] A. Kitaev (2014), talks given at the Fundamental Physics Prize Symposium, Nov. 10, 2014, and at KITP, Feb. 12, 2015.
[12] J. S. Cotler, G. Gur-Ari, M. Hanada, J. Polchinski, P. Saad, S. H. Shenker, D. Stanford, A. Streicher, and M. Tezuka, J. High Energy Phys. 05 (2017) 118.
[13] O. Bohigas, M. J. Giannoni, and C. Schmit, Phys. Rev. Lett. **52**, 1 (1984).
[14] See, e.g., Refs. [5,12].
[15] For the other two symmetry classes the detailed shape of this growth segment has similar features, but the details are slightly different.
[16] The plotted data are actually for the reduced density matrix of a typical one-dimensional Floquet many-body system to be discussed in Sec. II C 1 and in Fig. 3 of the main text, but this is not relevant for the current discussion.
[17] See detailed discussions below (2.1), (2.2), (2.3).
[18] M. Berry, Proc. R. Soc. Lond. A **400**, 229 (1985).
[19] J. H. Hannay and A. M. Ozorio De Almeida, J. Phys. A: Math. Gen. **17**, 3429 (1984).
[20] M. C. Gutzwiller, *Chaos in Classical and Quantum Mechanics* (Springer, New York, 1990).
[21] S. Sachdev and J. Ye, Phys. Rev. Lett. **70**, 3339 (1993).
[22] A. Kitaev (2015), talks at KITP, April 7, 2015 and May 27, 2015.
[23] J. Maldacena and D. Stanford, Phys. Rev. D **94**, 106002 (2016).
[24] P. Forrester, *Log-Gases and Random Matrices (LMS-34)* (Princeton University Press, Princeton, NJ, 2010).
[25] Since we consider systems without time-reversal symmetry.
[26] J. R. Garrison and T. Grover, Phys. Rev. X **8**, 021026 (2018).
[27] D. N. Page, Phys. Rev. Lett. **71**, 1291 (1993).
[28] A. I. Larkin and Yu. N. Ovchinnikov, JETP **28**, 1200 (1969).
[29] M. Rigol, V. Dunjko, V. Yurovsky, and M. Olshanii, Phys. Rev. Lett. **98**, 050405 (2007).
[30] M. Rigol, A. Muramatsu, and M. Olshanii, Phys. Rev. A **74**, 053616 (2006).
[31] P. Calabrese and J. Cardy, J. Stat. Mech. (2007) P06008.
[32] J. Cardy, J. Stat. Mech. (2016) 023103.
[33] T. Mori, T. Kuwahara, and K. Saito, Phys. Rev. Lett. **116**, 120401 (2016).
[34] D. A. Abanin, W. De Roeck, and F. Huveneers, Phys. Rev. Lett. **115**, 256803 (2015).
[35] D. A. Abanin, W. De Roeck, W. W. Ho, and F. Huveneers, Phys. Rev. B **95**, 014112 (2017).
[36] D. V. Else, B. Bauer, and C. Nayak, Phys. Rev. X **7**, 011026 (2017).
[37] Z.-C. Yang, A. Hamma, S. M. Giampaolo, E. R. Mucciolo, and C. Chamon, Phys. Rev. B **96**, 020408 (2017).

[38] S. D. Geraedts, R. Nandkishore, and N. Regnault, Phys. Rev. B **93**, 174202 (2016).
[39] M. Mierzejewski, T. Prosen, D. Crivelli, and P. Prelovšek, Phys. Rev. Lett. **110**, 200602 (2013).
[40] In the present paper we often follow the notations used in Ref. [12].
[41] See, e.g., Ref. [5] for an extensive review.
[42] R. E. Prange, Phys. Rev. Lett. **78**, 2280 (1997).
[43] V. Balasubramanian, B. Craps, B. Czech, and G. Sárosi, J. High Energy Phys. 3 (2017) 154.
[44] These oscillations can be systematically reduced by averaging over larger samples.
[45] We actually studied $\langle ZZ^* \rangle$ for eigenstates in both Floquet and Ising models with $L = 14$ and we can observe a smaller linear ramp in it.
[46] H. Kim, T. N. Ikeda, and D. A. Huse, Phys. Rev. E **90**, 052105 (2014).
[47] A. Lazarides, A. Das, and R. Moessner, Phys. Rev. E **90**, 012110 (2014).
[48] P. Ponte, A. Chandran, Z. Papić, and D. A. Abanin, Ann. Phys. **353**, 196 (2015).
[49] L. Zhang, H. Kim, and D. A. Huse, Phys. Rev. E **91**, 062128 (2015).
[50] M. C. Bañul, J. I. Cirac, and M. B. Hastings, Phys. Rev. Lett. **106**, 050405 (2011).
[51] We choose here the 10 largest eigenvalues, of a total of approx. $N_A = 500$ levels of $\hat{\rho}_A$.
[52] We choose here the 10 smallest eigenvalues, of a total of approx. $N_A = 500$ levels of $\hat{\rho}_A$.
[53] See the last paragraph before Sec. III C and Fig. 9.
[54] L. D'Alessio and A. Polkovnikov, Ann. Phys. **333**, 19 (2013).
[55] F. Machado, G. D. Meyer, D. V. Else, C. Nayak, and N. Y. Yao, arXiv:1708.01620.
[56] See, e.g., Ref. [61] and references therein.
[57] T. Nagao and M. Wadati, J. Phys. Soc. Jpn. **61**, 78 (1992).
[58] E. Brézin and A. Zee, Nucl. Phys. B **402**, 613 (1993).
[59] D. Fox and P. B. Kahn, Phys. Rev. **134**, B1151 (1964).
[60] From (4.11) the number ΔN of levels λ_i that lie in the interval $[\lambda - \Delta\lambda/2, \lambda + \Delta\lambda/2]$ is $\Delta N = \int_{\lambda-\Delta\lambda/2}^{\lambda+\Delta\lambda/2} \langle \hat{\nu}(\lambda') \rangle d\lambda' \approx \langle \hat{\nu}(\lambda) \rangle \Delta\lambda$, so that the local density of levels and thus the inverse of the local mean level spacing is $\langle \hat{\nu}(\lambda) \rangle = 1/(\Delta\lambda/\Delta N) = 1/\overline{(\delta\lambda)}$, where $\overline{(\delta\lambda)} = (\Delta\lambda/\Delta N)$ denotes the local level spacing near the eigenvalue λ.
[61] B. Bertini, F. H. L. Essler, S. Groha, and N. J. Robinson, Phys. Rev. B **94**, 245117 (2016).